Insights into the involvement of spliceosomal mutations in myelodysplastic disorders from an analysis of SACY-1/DDX41 in *Caenorhabditis elegans*

Tatsuya Tsukamoto,*[,1] Micah D. Gearhart,*[,1] Seongseop Kim,*[,1,2] Gemechu Mekonnen,* Caroline A. Spike,* and David Greenstein*[,3]

*Department of Genetics, Cell Biology and Development, University of Minnesota, Minneapolis, Minnesota 55455, USA

Running title: Genetic analysis of DDX41 in *C. elegans*

Keywords: SACY-1/DDX-41, spliceosome, myelodysplastic disorders, *C. elegans*

[1]These authors contributed equally to this work.

[2]Present address: OriGene Technologies Inc., 9620 Medical Center Drive, Suite 200, Rockville, MD 20850

[3]Corresponding author: David Greenstein, Department of Genetics, Cell Biology, and Development, University of Minnesota, 4-208 MCB, 420 Washington Avenue SE, Minneapolis, MN 55455. Tel: 612-624-3955; FAX: 612-626-6140. E-mail: green959@umn.edu

Manuscript Details

Tables: 6

Figures: 7

Words: 16,107

References: 104

Supplemental Information (submitted to FigShare)

Supplemental Tables: 5

Supplemental Figures: 8

Supplemental Files: 3

Supplemental Figure Legends

Author Summary

Mutations affecting spliceosomal proteins are frequently found in hematological malignancies. DDX41/Abstrakt is a metazoan-specific spliceosomal DEAD-box RNA helicase recurrently mutated in inherited and relapsing myelodysplastic syndromes and acute myeloid leukemia. The genetic properties and genomic impacts of disease-causing mutations in spliceosomal proteins have been uncertain. Here we conduct a comprehensive molecular genetic analysis of the *C. elegans* DDX41 ortholog, SACY-1. Our results reveal that multiple *sacy-1/DDX41* missense mutations, including the R525H human oncogenic variant, exhibit antimorphic activity that likely compromises the function of the spliceosome. The genomic consequences of SACY-1 depletion include splicing- splicing-independent and splicing-dependent alterations in the transcriptome.

ABSTRACT

Mutations affecting spliceosomal proteins are frequently found in hematological malignancies, including myelodysplastic syndromes and acute myeloid leukemia. DDX41/Abstrakt is a metazoan-specific spliceosomal DEAD-box RNA helicase found to be recurrently mutated in inherited myelodysplastic syndromes and in relapsing cases of acute myeloid leukemia. The genetic properties and genomic impacts of disease-causing missense mutations in DDX41 and other spliceosomal proteins have been uncertain. Here we conduct a comprehensive molecular genetic analysis of the *C. elegans* DDX41 ortholog, SACY-1. Our results reveal general essential functions for SACY-1 in both the germline and the soma, as well as specific functions affecting germline sex determination and cell cycle control. Certain *sacy-1/DDX41* mutations, including the R525H human oncogenic variant, confer antimorphic activity, suggesting that they compromise the function of the spliceosome. Consistent with these findings, *sacy-1* exhibits synthetic lethal interactions with several spliceosomal components, and biochemical analyses suggest that SACY-1 is a component of the *C. elegans* spliceosome. We used the auxin-inducible degradation system to analyze the impact of SACY-1 on the transcriptome using RNA sequencing. SACY-1 depletion impacts the transcriptome through splicing-independent and splicing-dependent mechanisms. The observed transcriptome changes suggest that disruption of spliceosomal function induces a stress response. Altered 3' splice site usage represents the predominant splicing defect observed upon SACY-1 depletion, consistent with a role for SACY-1 as a second-step splicing factor. Missplicing events appear more prevalent in the soma than the germline, suggesting that surveillance mechanisms protect the germline from aberrant splicing.

INTRODUCTION

Mutations affecting components of the spliceosome are frequently found in hematological malignancies, including myelodysplastic syndromes (MDS; Yoshida *et al*. 2011; reviewed by Yoshida and Ogawa 2014; Coltri *et al*. 2019), which comprise a heterogeneous set of myeloid neoplasms characterized by anemia and cytopenia that progress to acute myeloid leukemia (AML) to varying degrees (Tefferi and Vardiman 2009). The genetic properties and genomic impacts of disease-causing missense mutations in DDX41 and other spliceosomal proteins have been uncertain. Nonetheless, mutations affecting spliceosomal components are predictive of poor clinical outcomes in AML patients (Papaemmanuil *et al.* 2016). Exactly how mutations in spliceosomal components contribute to malignancy is uncertain, but an attractive model is that aberrant splicing may interrupt tumor suppressor activity. Importantly, genome sequencing data in patients is currently being used in the clinic to generate personalized prognoses, with the idea of optimally targeting existing therapies and generating new treatment strategies (Grinfeld *et al*. 2018). One potential therapeutic approach under development is the discovery of splicing inhibitors (Effenberger *et al*. 2017; Kim and Abdel-Wahab 2017; DeNicola and Tang 2019). Although mutations affecting several spliceosomal proteins appear to be beneficial to tumor cells, excessive splicing abnormalities are likely to be lethal to all cells. Splicing inhibitors have been demonstrated to target tumor cells with splicing mutations by inducing excessive splicing abnormalities, but cells with intact splicing machinery appear to be resistant to these agents (Seiler *et al*. 2018). In fact, several new splicing inhibitors are currently in clinical trials.

The spliceosomal components frequently affected in MDS include the biochemically well-defined factors SF3B1, SRSF2, and U2AF1 (Yoshida *et al*. 2011; reviewed by Yoshida and Ogawa 2014). More recent studies have implicated DDX41 (Ding *et al*. 2012; Lewinsohn *et al*. 2015; Polprasert *et al*. 2015; Cardoso *et al*. 2016; Li *et al*. 2016; Diness *et al.* 2018; reviewed by Maciejewski *et al*. 2017), a DEAD-box RNA helicase highly conserved in metazoans, whose precise biochemical function in the spliceosome is less well understood. DDX41 appears to be specifically recruited to the

87 catalytically active C complex (Jurica *et al*. 2002; Bessonov *et al*. 2008), which performs the second
88 step of splicing in which the 5' and 3' exons are ligated and an intronic lariat is released. DDX41 is
89 one of many spliceosomal proteins specific to metazoans and not found in budding yeast (Bessonov *et*
90 *al*. 2008).

91 Whole genome sequencing studies suggest that *DDX41* mutations are associated with
92 hematological malignancies that are considered to be different clinical entities. For example,
93 examination of clonal evolution of relapsed AML cases identified *DDX41* as one of several genes
94 found to be mutated in secondary tumors but not the primary tumors, suggesting it plays a role as a
95 tumor suppressor and might be causative for disease progression (Ding *et al*. 2012). By contrast,
96 studies of familial acute myeloid leukemia syndromes suggest that preexisting germline *DDX41*
97 mutations in trans to newly arising somatic mutations cause the development of hematological
98 malignancies (Polprasert *et al*. 2015; Cardoso *et al*. 2016; Lewinsohn *et al*. 2016; Li *et al*. 2016).
99 Germline biallelic *DDX41* missense mutations were recently reported in two siblings that exhibited
100 intellectual disability, psychomotor delays, and facial and skeletal dysmorphologies, with one sibling
101 presenting with childhood leukemia (Diness *et al*. 2018). Other work suggests that DDX41 might be a
102 multifunctional protein; in addition to its nuclear function in RNA splicing, it has been suggested to
103 function as a cytoplasmic DNA sensor in a signaling pathway in the cytoplasm that detects infecting
104 double stranded DNA and initiates an antiviral interferon response (Zhang *et al*. 2011; Parvatiyar *et al*.
105 2012; Stavrou *et al*. 2015, 2018; reviewed by Jiang *et al*. 2017). However, more recent work suggests
106 that cyclic GMP-AMP synthase (cGAS) functions as the major DNA sensor and is several orders of
107 magnitude more effective in inducing interferon beta synthesis than DDX41 (Sun *et al*. 2013). Two
108 studies, one of DDX41 and another of its *Drosophila* ortholog, Abstrakt, suggested a role in regulating
109 translation of the cyclin-dependent kinase inhibitor $p21^{WAF1/CIP1}$ (Peters *et al*. 2017) and the Inscuteable
110 protein (Irion *et al.* 2004), respectively, though the exact mechanism for these activities has not been
111 elucidated and indirect effects acting at the level of splicing were not addressed in these studies.

To better understand the highly conserved functions of *DDX41*, we undertook a comprehensive molecular genetic analysis of its ortholog, *sacy-1* in the nematode *Caenorhabditis elegans*. Our prior studies identified the DEAD-box helicase SACY-1 as a negative regulator of oocyte meiotic maturation functioning in the germline upstream of the TIS11 CCCH zinc-finger RNA-binding proteins OMA-1 and OMA-2 (Kim *et al.* 2012). Genetic analysis also established roles for SACY-1 in regulating the hermaphrodite sperm-to-oocyte switch and in preventing necrotic cell death of gametes. Genetic experiments further suggested an essential role for *sacy-1(+)* in early embryos and larvae that appeared to be maternally rescued. At the time of our original study, searchable databases of the scientific literature had not yet annotated DDX41 (or its *Drosophila* ortholog, Abstrakt) as spliceosomal components identified by proteomics. We therefore did not recognize that SACY-1 was likely involved in splicing.

In this study, we undertook a comprehensive molecular genetic analysis of SACY-1's functions in *C. elegans*. Our results are most consistent with an essential role for SACY-1 in spliceosome function. Further, our genetic results reveal that certain *sacy-1* mutations appear to confer a dosage-sensitive antimorphic activity, most consistent with the possibility that they compromise the function of the spliceosome by perturbing the function of other spliceosomal proteins. The oncogenic R525H mutation in human DDX41 was introduced into the *C. elegans* genome using CRISPR-Cas9 genome editing and found to exhibit weak antagonistic activity. Consistent with these findings, *sacy-1* exhibits genetic interactions with associated spliceosomal components, and biochemical analyses suggest that SACY-1 is a component of the *C. elegans* spliceosome. Depletion of SACY-1 in the germline or soma was found to have major impacts on the transcriptome through splicing-independent and splicing-dependent mechanisms. Alterations in 3' splice site selection represent the most prevalent changes in splicing patterns observed following SACY-1 depletion, consistent with its function as a component of the spliceosomal C complex. Missplicing events are more prevalent upon SACY-1 depletion in the soma than in the germline, leading us to suggest that surveillance mechanisms protect the germline

from aberrant splicing. The observed gene expression changes observed after SACY-1 depletion suggest that perturbations of spliceosomal function might induce a stress response. Our results, taken together with a recent study of *sftb-1/SF3B1* (Serrat *et al*. 2019), highlight the potential of the *C. elegans* system for examining the molecular genetic properties of disease-causing mutations affecting highly conserved components of the spliceosome.

MATERIALS AND METHODS

C. elegans strains and genetic analysis

The genotypes of strains used in this study are reported in Supporting Information, Table S1. Genes and mutations are described in WormBase (www.wormbase.org; Harris *et al*. 2013) or in the indicated references. Culture and genetic manipulations were conducted at 20°C unless specified otherwise. The following mutations were used: LGI– *fog-1(q253*ts*)*, *dpy-5(e61)*, *gld-1(tn1478)*, *unc-13(e51)*, *unc-13(e1091)*, *lin-41(n2914)*, *lin-41(tn1541[gfp::tev::s-tag::lin-41])*, *sacy-1(tm5503)*, *sacy-1(tn1385)*, *sacy-1(tn1479)*, *sacy-1(tn1480)*, *sacy-1(tn1481*Mog*)*, *sacy-1(tn1482)*, *sacy-1(tn1602)*, *sacy-1(tn1603)*, *sacy-1(tn1604)*, *sacy-1(tn1605)*, *sacy-1(tn1606)*, *sacy-1(tn1607)*, *sacy-1(tn1608)*, *sacy-1(tn1609)*, *sacy-1(tn1610)*, *sacy-1(tn1611)*, *sacy-1(tn1612)*, *sacy-1(tn1615)*, *sacy-1(tn1616)*, *sacy-1(tn1617)*, *sacy-1(tn1632[3xFLAG::PreScission protease site::gfp::tev::s-tag::sacy-1])*, *sacy-1(tn1880[aid::gfp::tev::myc::sacy-1])*, and *sacy-1(tn1887)*; LGII–*tra-2(e2020)*, *ieSi57[eft-3p::TIR1::mRuby::unc-54 3'UTR + Cb unc-119(+)], ieSi64[gld-1p::TIR1::mRuby::gld-1 3'UTR + Cb unc-119(+)]*; LGIII–*unc-119(ed3)*; LGIV–*unc-24(e138)*, *fem-3(e1996)*, and *dpy-20(e1282)*; LGV–*acy-4(ok1806)*, *her-1(hv1y101)*, *emb-4(sa44)*, *unc-51(e369)*, and *fog-2(oz40)*. The following rearrangements were used: *hT2[bli-4(e937) let-?(q782) qIs48]* (I;III), *tmC18[dpy-5(tmIs1236) + pmyo-2::mCherry]* I (Dejima *et al*. 2018), *mIn1[dpy-10(e128) mIs14]* II, and *tmC12[egl-9(tmIs1194) + pmyo-2::Venus]* V (Dejima *et al*. 2018). The following transgenes were used: *tnEx37[acy-4(+) + sur-5::gfp]*, *tnEx159[gfp:sacy-1 + pDPMM0016B(unc-119(+))]*.

For the analysis of genetic interactions between *sacy-1(tn1481)* and *fem-3(e1996)*, non-Unc non-Dpy non-GFP animals from *sacy-1(tn1481)/hT2[bli-4(e937) let-?(q782) qIs48]; fem-3(e1996)/unc-24(e138) dpy-20(e1282)* were individually cultured and scored for germline phenotypes. Following scoring, the *fem-3* genotype of each animal was scored by conducting PCR with primers *fem-3* F2 and *fem-3* R2 and sequencing the products.

To map the cold-sensitive (15°C) and temperature-sensitive (25°C) phenotypes of *sacy-1(tn1480)*, 34 Unc non-Dpy recombinants were obtained from *sacy-1(tn1480)/dpy-5(e61) unc-13(e1091)* heterozygotes. The recombinant chromosomes were bred to homozygosity and scored for the presence or absence of the *sacy-1(tn1480)* mutation by conducting PCR with primers H27M09.1F1 and H27M09.1R4 and sequencing purified PCR products with primer H27M09.1F2. We found that 7 of the 34 recombinants contained *sacy-1(tn1480)* and were cold-sensitive and temperature-sensitive. By contrast, 27 recombinants were *sacy-1(+)* and grew at 15°C and 25°C. These data indicate that *sacy-1(tn1480)* mutation is inseparable from the cold-sensitive and temperature-sensitive phenotypes (e.g., within ~0.06 map units). In addition, 32 Dpy non-Unc recombinants were selected. Interestingly, all the homozygous recombinants were fertile at both 15°C and 25°C, including the 22 recombinants that contained the *sacy-1(tn1480)* mutation. Although these *dpy-5(e61) sacy-1(tn1480)* recombinants grew at 15°C and 25°C, they produced appreciable numbers of dead embryos and grew more slowly than their *sacy-1(+)* counterparts. This result suggests that the *dpy-5(e61)* mutation suppresses the cold-sensitive and temperature-sensitive phenotypes of *sacy-1(tn1480)*. Previous work has shown that mutant alleles of collagen genes can suppress temperature-sensitive mutations in other gene products possibly by triggering a stress response (Levy *et al*. 1993; Maine and Kimble 1993; Nishiwaki and Miwa 1998). That *dpy-5(e61)* suppresses *sacy-1(tn1480)* was further shown by constructing *dpy-5(e61) sacy-1(tn1480)/sacy-1(tn1480) unc-13(e1091)* heterozygotes (n=30), of which 20 exhibited the *sacy-1(tn1480)* sperm-defective phenotype at 25°C and 10 were fertile. Thus, *dpy-5(e61)* exhibits semidominance for its effects on body morphology and for suppression of *sacy-1(tn1480)*. To examine the dominant Him phenotype of *sacy-1(tn1480)* and its interaction with *sacy-1(tn1887)*, we compared the percentage of males produced at 25°C by *dpy-5(e61)/sacy-1(tn1480) unc-13(e1091)* and *dpy-5(e61) sacy-1(tn1887)/sacy-1(tn1480) unc-13(e1091)* heterozygotes.

RNA interference

Genome-wide RNA interference (RNAi) screening employed the Ahringer feeding library (Kamath *et al*. 2003) using the RNAi culture media described by Govindan *et al*. (2006) at 22°C. The empty vector L4440 was used as a control. The identity of RNAi clones was verified by DNA sequencing. Gene-specific RNAi was performed by placing gravid hermaphrodites on RNAi medium seeded with double-stranded RNA (dsRNA)-expressing *E. coli* (Timmons and Fire 1998). The gravid hermaphrodites were immediately treated with 20% bleach to release the F1 embryos. Phenotypes were assessed 3–4 days later. For quantification of phenotypes, sterility and gamete degeneration were scored in the F1 generation, and embryonic lethality was scored in the F2 generation produced by the RNAi-treated F1 animals.

Immunofluorescence, fluorescent labeling, and microscopy

Dissected gonads were fixed in 3% paraformaldehyde as described (Rose *et al.* 1997). Fixed gonads were stained with rabbit anti-RME-2 antibody (Grant and Hirsh 1999; kindly provided by B. Grant, Rutgers University, 1:50), a mixture of two purified mouse monoclonal anti-MSP antibodies (Kosinski *et al.* 2005, each at 1:300), rabbit anti-phospho-histone H3 (Ser10) antibody (Millipore, 1:400). Secondary antibodies were Alexa 488-conjugated donkey anti-rabbit antibodies (Jackson ImmunoResearch, 1:500) and Cy3-conjugated goat anti-mouse antibodies (Jackson ImmunoResearch, 1:500). 4', 6-diamidino-2-phenylindole (DAPI) was used to detect DNA. DIC and fluorescent images were acquired on a Zeiss motorized Axioplan 2 microscope with either a 40x Plan-Neofluar (numerical aperture 1.3) or a 63x Plan-Apochromat (numerical aperture 1.4) objective lens using a AxioCam MRm camera and AxioVision software (Zeiss).

Genome editing

CRISPR-Cas9 genome editing used pRB1017 to express single guide RNA (sgRNA) under control of the *C. elegans* U6 promoter (Arribere *et al*. 2014). The sequences of all oligonucleotides used are listed in Table S2. To generate sgRNA clones, annealed oligonucleotides were ligated to *Bsa*I-digested pRB1017 plasmid vector, and the resulting plasmids were verified by Sanger sequencing. pDD162 served as the source of Cas9 expressed under control of the *eef-1A.1/eft*-3 promoter (Dickinson *et al*. 2013). Indels were targeted to exon 2 of *sacy-1* using *sacy-1* sgRNA7 (pCS520). The injection mix contained pCS520 (25 ng/µl), pDD162 (50 ng/µl), and *Pmyo-2::tdTomato* (4 ng/µl). *sacy-1(tn1602–tn1612)* were recovered from injections into DG3913 *lin-41(tn1541[gfp::tev::s-tag::lin-41])* and *sacy-1(tn1615–1617)* were recovered from injections into the wild type (strain N2).

An N-terminal *gfp* fusion to endogenous *sacy-1*, *sacy-1(tn1632[3xflag::PreScission protease site::gfp::tev::s-tag::sacy-1]),* was constructed using *sacy-1* sgRNA1 (pCS486) and a repair template generated by conducting the PCR with oligonucleotide primers *sacy-1* 5HAF and *sacy-1* 3HAR, using a *gfp::sacy-1::tev::s-tag* recombineered fosmid (SK212; Kim *et al*. 2012) as template. Genome editing employed the *dpy-10* co-conversion method (Arribere *et al.* 2014). The injection mix contained pJA58 (7.5 ng/µl), AF-ZF-827 (500 nM), pCS486 (50 ng/µl), repair template (50 ng/µl), and pDD162 (50 ng/µl) and was injected into wild-type worms. Correct targeting was verified by conducting PCR with primer pairs GFP_7215 and H27M09.1_R5 and GFP_1094R and H27M09.1_seqF1 followed by DNA sequencing.

An N-terminal auxin-inducible degron (aid) fusion to *sacy-1*, *sacy-1(tn1880[aid::gfp::myc::sacy-1]),* was constructed using *sacy-1* sgRNA1 and a repair template generated by conducting the PCR with oligonucleotide primers *sacy-1* AID5F and *sacy-1* AID3R using a *wee-1.3::aid::gfp::myc* clone (pCS575, C. Spike, unpublished results) as template. The injection mix was prepared as described above and was injected into CA1352 worms. *sacy-1* (*sacy-1(tn1880[aid::gfp::myc::sacy-1])* was identified by screening the progeny of 414 F1 Roller animals for

GFP fluorescence. Correct targeting was verified by conducting PCR with primer pairs GFP_R1 and H27M09.1_F5 and GFP_F1 and H27M09.1_R5 followed by DNA sequencing.

The R525H mutation in DDX41 was imported into *C. elegans* (e.g., SACY-1[R534H]) using genome editing (Paix *et al.* 2014) with *sacy-1* sgRNA11 and *sacy-1* sgRNA12 and a single-stranded repair oligonucleotide (*sacy-1* GM1), which introduces the R534H mutation and two synonymous changes to alter the protospacer adjacent motif and to facilitate screening using an introduced *Ava*I restriction site. The injection mix contained pJA58 (7.5 ng/µl), AF-ZF-827 (500 nM), *sacy-1* sgRNA11 (25 ng/µl), *sacy-1* sgRNA12 (25 ng/µl), *sacy-1* GM1 (500 nM), and pDD162 (50 ng/µl) and was injected into wild-type worms. Edited loci were verified by PCR and DNA sequencing using primers sacy-1 seq F1 and sacy-1 seq R1.

Antibody production, purification, and western blotting

sacy-1 cDNA sequences were cloned into the *E. coli* expression vector pMal-c2 to create an inducible fusion protein wherein maltose binding protein was fused to amino acids 411–578 of SACY-1 (MBP::SACY-1(411–578)). MBP::SACY-1(411–578) was column and gel-purified and used to immunize rabbits. Immunizations and sera collection were performed using standard protocols (Cocalico Biologicals, Inc., Reamstown, PA). Rabbit antibody (R217) was affinity purified and was suitable in western blots with partially purified SACY-1 preparations. Hybridoma cell lines producing anti-GFP monoclonal antibodies 12A6 and 4C9 (Sanchez *et al*. 2014) were obtained from the Developmental Studies Hybridoma Bank and prepared as described (Tsukamoto *et al*. 2017). Proteins were separated using NuPAGE 4-12% Bis-Tris gels (Invitrogen) and visualized after western blotting. Blots were blocked with 5% nonfat dried milk. Primary antibodies used to detect proteins were affinity-purified rabbit anti-SACY-1(411–578) R217 antibody (100 ng/ml) and rabbit anti-GFP NB600-308 antibody (Novus Biologicals; 250 ng/ml). The secondary antibody used for western blots was peroxidase-conjugated donkey anti-rabbit antibody (Jackson ImmunoResearch; 1:30,000).

Detection was performed using SuperSignal West Femto Maximum Sensitivity Substrate (Thermo Scientific).

SACY-1 tandem affinity purification

Tandem affinity purification of SACY-1 was conducted using strains DG4068 and DG4070 using modifications of a previously described protocol (Tsukamoto *et al.* 2017). Immunopurified proteins were precipitated with 16.7% trichloroacetic acid (TCA), washed with acetone at –20°C, and briefly separated on a 12% NuPAGE Bis-Tris gel, stained with Colloidal Blue Staining Kit (Invitrogen). Lanes were subdivided into eight gel slices and mass spectrometry was performed at the Taplin Biological Mass Spectrometry Facility (Harvard Medical School) using an LTQ Orbitrap Velos Pro ion-trap mass spectrometer (Thermo Fisher Scientific). Protein identification used the Sequest software program (Thermo Fisher Scientific) to match the fragmentation pattern of tryptic peptides to the *C. elegans* proteome. The data were filtered to a 1–2% peptide false discovery rate. File S1 reports the mass spectrometry results and the additional filtering criteria for identifying non-specific interactions.

RNA sequencing

The auxin-inducible degradation system (Zhang *et al*. 2015) was used to deplete SACY-1 using strain backgrounds in which TIR1 was expressed in the germline (CA1352) or soma (CA1200). Experimental (DG4700 and DG4703) and control strains (CA1352 and CA1200) were grown on peptone-enriched nematode growth medium with NA22 as a food source. Embryos were isolated by alkaline hypochlorite treatment (20% bleach and 0.5 N NaOH), washed in M9 buffer and allowed to hatch overnight in the absence of food. For each of three biological replicates, 60,000 L1-stage larvae were cultured on two 150- by 15-mm petri dishes containing peptone-enriched medium with OP50. The worms were grown to the young adult stage and harvested by washing off the plates with M9 and then placed on fresh plates containing peptone-enriched medium and 2 mM auxin seeded with OP50.

Plates were cultured in the dark at 20°C for 24 hours. The worms were then harvested and washed with M9 repeatedly to reduce the presence of *E. coli*. Total RNA was isolated using TRIzol LS Reagent (Invitrogen, Carlsbad, CA) and the RNAeasy Micro Kit (QIAGEN, Valencia, CA). Poly(A)+ RNA was selected from 1 µg of total RNA using the NEBNext Ultra Kit (New England Biolabs, Ipswitch, MA). Libraries were prepared and sequenced by Genewiz (South Plainfield, NJ). Paired-end reads of 150 base pairs (bp) were obtained on an Illumina HiSeq4000 instrument with an average depth greater than 31 million reads per sample.

Bioinformatics

After trimming adapters with Trim Galore (v0.6.0) and cutadapt (v1.18), reads were assessed for quality with FastQC (v0.11.8), mapped to the WBcel235/ce11 genome with STAR (v2.7.2a) guided by gene annotations defined in Ensembl (release 97) and sorted and indexed with samtools (v1.7). Gene-level abundance was estimated for Ensembl defined annotations using the featureCounts function in the Bioconductor package Rsubread (v1.28.1). An average of 28 million high-quality (MAPQ > 55) reads mapped to annotated genes within each sample. Principal component analysis and inspection of 5' vs 3' read coverage indicated that one soma control sample (CA1200-2) contained degraded RNA and was excluded from further analysis. Differential gene expression of Ensembl defined genes was determined using DESeq2 (v1.26.0). P values were adjusted for multiple test correction using Benjamini–Hochberg procedure. The fold change, adjusted p values, the mean number of counts across samples and the number of complementary DNA fragments per kilobase of transcript per million mapped reads (FPKM) were used to define differentially expressed genes. Gene ontology (GO) data were obtained from WormBase release WS273 and analyzed taking length bias into account using the Goseq (v1.38.0) package. Novel transcripts in each of the high quality samples and in the previously published GSE57109 (Ortiz *et al*. 2014) dataset were identified using StringTie (v2.0.4) and merged together with the Ensembl annotations to generate a comprehensive annotation set. These annotations

were used with RMATS (v4.0.2 turbo) to determine statistically significant differences for splicing events between conditions [expressed as false discovery rates (FDRs)]. Coverage data was visualized with Gviz (v 1.30.0). A custom R script with details for the analysis and figure generation is available at https://github.com/micahgearhart/sacy1.

Data availability

Strains and reagents are available upon request. RNA sequencing data have been deposited in NCBI's Gene Expression Omnibus and are accessible through accession number XXXX.

RESULTS

Synthetic lethal interactions between a sacy-1 reduction-of-function allele and several genes encoding spliceosomal proteins

In prior studies, we recovered reduction-of-function (rf) *sacy-1* mutant alleles as suppressors of *acy-4* sterility (Kim *et al*. 2012). ACY-4 is an adenylate cyclase that functions in the gonadal sheath cells to promote oocyte growth and meiotic maturation (Govindan *et al*. 2009; Nadarajan *et al*. 2009). *acy-4* null mutants are sterile, whereas *sacy-1(*rf*); acy-4(0)* mutants are fertile, and this suppression was shown to involve reduced *sacy-1* function in the germline (Kim *et al*. 2012). *sacy-1(*rf*)* mutants were also found to suppress the self-sterility of *fog-2* null mutants that results from a failure to produce sperm. A sperm-to-oocyte switch governs hermaphrodite germline sex determination. In wild-type hermaphrodites, the first differentiating germ cells produce sperm in the L4 larval stage, whereas, later differentiating germ cells exclusively produce oocytes in the adult stage. The suppression of *fog-2* sterility suggested that *sacy-1* has a function to promote the oocyte fate. Analysis of the *sacy-1(tm5503)* deletion allele, which is a likely null allele (see below), indicated that *sacy-1* also functions to prevent necrotic degeneration of sperm and oocytes and is required for fertility of hermaphrodites and males (Kim *et al.* 2012).

To better understand the function of *sacy-1* in multiple germline processes, we conducted a genome-wide RNAi screen for loci that enhance *sacy-1* mutant phenotypes, such as sterility or embryonic lethality. Specifically, we screened for loci which caused severe phenotypes when knocked down by RNAi in the *sacy-1(tn1385*rf*)* genetic background but not in the wild type. We screened 18,101 RNAi clones from the Ahringer RNAi library and identified five clones that enhanced *sacy-1* mutant phenotypes when they are knocked down (Table 1). The five RNAi clones target the transcripts of three genes (Table 1): *mog-2* (one clone), *Y111B2A.25* (one clone), and *emb-4* (three clones). To test whether *sacy-1* expression and/or localization is affected by RNAi of *mog-2*, *Y111B2A.25*, or *emb-4*, we conducted RNAi of these genes in *sacy-1(tm5503)* mutant animals expressing the rescuing

gfp::sacy-1 transgene (*tnEx159*). In no case did we observe that an RNAi treatment altered the expression or localization of the GFP::SACY-1 transgene; the expression level and predominant nuclear localization of GFP::SACY-1 after RNAi was similar to that of the control animals (S. Kim and D. Greenstein, unpublished results). This result suggests that the RNAi treatments enhance *sacy-1(tn1385)* mutant phenotypes through effects independent of SACY-1 expression and localization.

mog-2(RNAi) induces a higher penetrance of sterility, gamete degeneration, and embryonic lethality in the *sacy-1(tn1385)* mutant genetic background in comparison to the wild type (Table 1; Figure S1). *mog-2* encodes the U2 snRNP protein A' (Zanetti *et al*. 2011), which is a constitutive component of the spliceosome (Jurica *et al*. 2002; Bessonov *et al*. 2008, 2010; Herold *et al*. 2009).

Similarly, *Y111B2A.25(RNAi)* specifically enhances the penetrance of multiple *sacy-1* mutant phenotypes, including sterility, gamete degeneration, and embryonic lethality (Table 1; Figure S1). *Y111B2A.25* is annotated as a pseudogene (Agarwal *et al*. 2010; www.wormbase.org). *Y111B2A.25* is part of an operon, and the expressed sequence tag (EST) data show that the *Y111B2A.25* locus is transcribed, but the transcript lacks protein-coding ability. In *C. elegans* ~40 bp of sequence identity is sufficient to induce off-target RNAi effects (Rual *et al*. 2007). Use of the Basic Local Alignment Search Tool (BLAST) indicates that *Y111B2A.25(RNAi)* might target the *cacn-1* locus, which encodes a spliceosomal protein and shares ~200 bp of sequence identity with *Y111B2A.25*. To test whether the enhanced sterility induced by *Y111B2A.25(RNAi)* in the *sacy-1(tn1385)* genetic background might be explained by an off-target effect to *cacn-1*, we conducted *cacn-1(RNAi)* and found that the *cacn-1(RNAi)* induces complete sterility in both the *sacy-1(tn1385)* and wild-type animals (Table 1 and Figure S1). Interestingly, under the *cacn-1(RNAi)* condition, the *sacy-1(tn1385)* animals show additional phenotypes, such as high penetrance of a protruding vulva (Pvl) phenotype and slow growth compared to the wild type, suggesting a genetic interaction between *cacn-1* and *sacy-1* that might be partially masked by the strong phenotypes induced by *cacn-1(RNAi)*. Thus, we reasoned that the short identity shared between *Y111B2A.25* and *cacn-1* dsRNA might induce strong sterility in the *sacy-*

*1(tn1385*rf*)* genetic background but not in the wild type through weaker interference with *cacn-1*. To test this possibility, we systematically reduced the efficacy of the *cacn-1(RNAi)* response by serially diluting the *cacn-1(RNAi)*-inducing bacteria with bacteria containing the empty vector control (L4440). Consistent with the possibility that *Y111B2A.25(RNAi*) targets *cacn-1*, limiting the efficacy of the *cacn-1(RNAi)* response revealed specific enhancement of sterility, gamete degeneration, and embryonic lethality in the *sacy-1(tn1385)* genetic background (Table S3). Notably, the response to limited *cacn-1(RNAi)* exhibited by *sacy-1(tn1385)* animals was remarkably similar to their response to *Y111B2A.25(RNAi)* (Table S3). The human and Drosophila orthologs of CACN-1 have been identified as components of spliceosomal C complexes (Jurica *et al*. 2002; Bessonov *et al*. 2008, 2010; Herold *et al*. 2009; Fica *et al*. 2019). Like DDX41/Abstrakt, Cactin is recruited to the C complex of the spliceosome.

In addition to *mog-2* and *Y111B2A.25*, we identified three different RNAi clones targeting the *emb-4* locus as strong enhancers of the *sacy-1(tn1385)* sterility and gamete degeneration phenotypes (Table 1; Figure S1). *emb-4* encodes a nuclear protein orthologous to human Aquarius/IBP160/KIAA0560/fSAP164, an intron-binding spliceosomal protein with a helicase-like domain (Sam *et al*. 1998; Jurica *et al*. 2002; Bessonov *et al.* 2008; Herold *et al*. 2009; De *et al*. 2015; Haselbach *et al*. 2018). To extend these RNAi results, we examined genetic interactions between *sacy-1* and *emb-4*, employing the *emb-4(sa44)* reduction-of-function allele. When combined with the *sacy-1(tm5503)* null allele, we observed enhancement of lethal vulval rupture and protruding vulva (Pvl) phenotypes in *sacy-1(tm5503); emb-4(sa44)* double mutants (Table 2A). We also observed enhancement of these phenotypes in *sacy-1(tn1385); emb-4(sa44)* double mutants, which were derived from *sacy-1(tn1385)/+; emb-4(sa44)* parents (Table 2A). Interestingly, the F1 progeny of fertile *sacy-1(tn1385); emb-4(sa44)* homozygous adults exclusively produced dead embryos or arrested L1-stage larvae, unlike each of the single mutants, which were highly fertile (Table 2B). Taken together these

genetic interactions between *sacy-1* and three genes encoding spliceosomal proteins suggest that multiple *sacy-1* mutant phenotypes might result from compromised functions of the spliceosome.

SACY-1 is a component of the C. elegans spliceosome

To characterize SACY-1-associated proteins, we conducted tandem affinity purifications using strains in which we used CRISPR-Cas9 genome editing to insert 3xFLAG and eGFP affinity tags at the SACY-1 N-terminus, separated by a PreScission protease recognition sequence (Figure S2). The resulting *sacy-1(tn1632[3x flag::PreScission::gfp::tev::s-tag::sacy-1])* strain was viable and fertile and exhibited no apparent germline or somatic defects. Although 3xFLAG::GFP::SACY-1 is expressed in all cells, it is particularly abundant in the female germline. Thus we conducted purifications from protein lysates prepared from adult animals in which the germline was feminized (experiment I) and also from adult hermaphrodites (experiment II). In both experiments, we found that 3xFLAG::GFP::SACY-1 associated with 55 proteins defined as spliceosomal proteins in other systems (Table 3; Jurica *et al*. 2002; Bessonov *et al*. 2008). The spliceosomal proteins identified in our genome-wide RNAi screen for *sacy*-1 enhancers (MOG-2, EMB-4, and CACN-1), were very well represented in our purifications (~35–56% peptide coverage; Table 3). We also detected 9 additional spliceosomal proteins in the purification from the female but not the hermaphrodite genetic background (Table S4), but this might be a consequence of the fact that more protein extract was used in that experiment. We also detected 28 other proteins in our tandem affinity purifications (Table S5). Homologs of several of these factors have been implicated in the regulation of RNA splicing, including NRDE-2 (Jiao *et al*. 2019), CIR-1 (Maita *et al*. 2005; Kasturi *et al*. 2010), and CDK-12 (Rodrigues *et al*. 2012). These biochemical studies, taken together with the results from the genome-wide RNAi screen, suggest that both specific and pleiotropic defects conferred by *sacy-1* mutant alleles might result from spliceosomal defects.

A sacy-1 reduction-of-function mutation enhances the Tumorous phenotype of a gain-of-function glp-1/Notch allele

Prior work showed that mutational or RNAi treatments affecting the function of multiple spliceosomal components could enhance weak gain-of-function (gf) mutations in *glp-1/Notch*, resulting in the ectopic proliferation of undifferentiated germ cells in the proximal gonad arm (Mantina *et al*. 2009; Kerins *et al*. 2010; Wang *et al*. 2012), which is referred to as a proximal proliferation or Tumorous phenotype. Thus, we constructed double mutants between the *sacy-1(tn1385)* mutation and the *glp-1(ar202*gf*)* mutation (Pepper *et al*. 2003). When analyzed in the young adult stage at 15°C (40 hrs post-L4), very few *glp-1(ar202*gf*)* adult hermaphrodites (~0.8%) were observed to exhibit a proximal proliferation phenotype with undifferentiated germ cells in the proximal gonad arm (Table 4). By contrast, many *sacy-1(tn1385*rf*); glp-1(ar202*gf*)* adults (~51%) exhibited a Tumorous phenotype (Table 4). This phenotype was not observed in *sacy-1(tn1385*rf*)* single mutants (Table 4). This result is consistent with the idea that the *sacy-1(tn1385*rf*)* mutation, though homozygous viable and fertile (brood size ~350; Kim *et al*. 2012), compromises the function of the spliceosome, as assessed in a sensitized genetic background.

Reduction-of-function sacy-1 mutations in C. elegans affect highly conserved residues in the DEAD-box and helicase domains

To better understand the functions and activities of the highly conserved SACY-1/DDX41 protein (Figure 1B), we conducted forward genetic screens for new *sacy-1* mutations, taking advantage of the fact that reductions of *sacy-1* function by mutation or RNAi can suppress the self-sterility of *fog-2* null mutations (Kim *et al*. 2012), which is caused by a failure to produce sperm (Schedl and Kimble 1988). Thus, we conducted a non-complementation screen for new mutations that enable fertility in trans to the *sacy-1(tn1385)* reduction-of-function allele in the *fog-2(oz40)* genetic background (Figure S3). In a screen of 15,577 haploid genomes, we isolated five new *sacy-1* missense alleles (*tn1479–tn1483*;

Figure 1; see Table 5 for a list of all *sacy-1* alleles central to this work and their properties). All the *sacy-1* missense mutations isolated thus far in *C. elegans* alter highly conserved amino acids, and several of these mutations are nearby or in subdomains of the DEAD-box affected by DDX41 mutations found in human neoplasms (Figure 1B). The *sacy-1* missense alleles were modeled onto the crystal structures of DEADc and the HELICc domains of DDX41 (Schütz *et al*. 2010; Omura *et al*. 2016) and found likely to be surface accessible (Figure 1C), suggesting that the mutant alleles might interfere with the function of other protein components of the spliceosome. Consistent with this idea, the non-complementation screen resulted in the isolation of three novel *sacy-1* alleles (*tn1479*, *tn1480*, and *tn1481*), which appear to confer antagonistic activities, likely at the level of the spliceosome (see below).

Similar to the *sacy-1(tm5503)* deletion allele which removes exons 2 and 3 and a portion of exon 4 (Figure 1A; Kim *et al*. 2012), *sacy-1(tn1479)* homozygous hermaphrodites were sterile and displayed the gamete degeneration phenotype, but with reduced penetrance (Table 6; Figure S4). Consistent with the idea that *sacy-1(tm5503)* defines the null phenotype, an antibody specific to a portion of the DEAD-box domain downstream of the *tm5503* deletion (residues 411–578) fails to detect a protein product in extracts from *sacy-1(tm5503)* adults (Figure S2). To further define the *sacy-1* null phenotype, we used CRISPR/Cas9 genome editing to generate indels upstream of the DEAD-box-encoding regions by targeting Cas9 double-strand DNA breaks to exon 2 with an efficient sgRNA. We generated *sacy-1* indels in both wild-type as well as *lin-41(tn1541[gfp::lin-41])* hermaphrodites, the latter serving to provide a marker for oocyte development (Spike *et al*. 2014a,b). In these experiments, we generated 14 new *sacy-1* alleles (*tn1602–tn1612* and *tn1615–tn1617*). Of these, 13 displayed the gamete degeneration phenotype, again consistent with this representing the null phenotype. Not surprisingly, GFP::LIN-41 levels declined and the protein became undetectable as oocytes degenerated (D. Greenstein, unpublished results). One of the new candidate null alleles, *sacy-1(tn1615)*, was sequenced and found to result from a 10 bp deletion at the end of exon 2, which is

predicted to introduce a stop codon prior to the DEAD-box domain, consistent with a null mutation (Figure 1B). Among the CRISPR-Cas9-induced alleles, *sacy-1(tn1617)* was exceptional in that it was homozygous viable and fertile, though slow growing, despite the fact that the deletion removes the initiation codon of *sacy-1* (Figure 1A). This exceptional allele might utilize an alternative start codon just prior to the DEAD-box domain, although this possibility was not explored. Since null mutations in *sacy-1* result in hermaphrodite sterility, there is the possibility that maternal *sacy-1(+)* activity contributes to the development of the germline and soma. Indeed, when the gamete degeneration phenotype is delayed through germline feminization, the mating of *sacy-1(tm5503)* null females to wild-type males produces embryos that arrest prior to morphogenesis (Kim *et al*. 2012).

One notable difference between *sacy-1(tn1479)* and the *sacy-1(tm5503)* null allele is that the majority of *sacy-1(tn1479*) adult hermaphrodites die by vulval rupture at 20°C (Table 6; Figure S4). This phenotype is only observed in a small minority of *sacy-1(tm5503)* hermaphrodites at 20°C but becomes the predominant phenotype at 15°C (Table 6). This observation suggests that *sacy-1(tn1479)* is more severe than a null allele, as might happen if the SACY-1[G504E] product is nonfunctional but also antagonizes a protein complex containing SACY-1, likely the spliceosome.

Unlike the *sacy-1(tm5503)* null allele, which is sterile, three of the newly isolated mutations *(tn1480*, *tn1482*, and *tn1483*) are self-fertile as homozygotes at 20°C similar to the *sacy-1(tn1385*rf*)* mutant. However, *sacy-1(tn1480)* and *sacy-1(tn1483)* homozygotes exhibited additional defects; both appeared to grow more slowly than the wild type at this temperature. In addition, *sacy-1(tn1483)* adult hermaphrodites had smaller gonad arms, suggesting effects on germline proliferation (T. Tsukamoto and D. Greenstein, unpublished results). Finally, *sacy-1(tn1480)* confers temperature-dependent gain-of-function pleiotropic defects that will be described below.

Novel sacy-1 mutant alleles appear to antagonize essential functions of the spliceosome

A recessive gain-of-function sacy-1 mutation masculinizes the hermaphrodite germline: In the non-complementation screen for *sacy-1* mutant alleles, we isolated a novel *sacy-1* allele, *tn1481*, with a masculinization of germline (Mog) phenotype (Table 6; Figure 2). All *sacy-1(tn1481)* homozygous hermaphrodites produce excess numbers of sperm but no oocytes (n=125). Staining of dissected gonads from adults showed that whereas all wild-type hermaphrodite gonad arms examined (n=64) expressed both the major sperm protein (MSP) and the RME-2 oocyte yolk receptor, all *sacy-1(tn1481)* gonad arms (n=178) expressed only MSP but not RME-2 (Figure 2). In our non-complementation screen (Figure S3), we also isolated a *gld-1* Mog allele, *tn1478*, as a dominant suppressor of *fog-2(oz40)*. *gld-1(tn1478)* results from the same G248R amino acid substitution reported for the *gld-1(q93)* Mog allele (Francis *et al*. 1995a,b; Jones and Schedl 1995). Thus it was important to determine whether the *sacy-1(tn1481*[P222L]*)* mutation was the cause of the Mog phenotype. This was ascertained by crossing a GFP::SACY-1 transgene (*tnEx159*) into the *sacy-1(tn1481)* genetic background. We found that all *sacy-1(tn1481); tnEx159 [gfp::sacy-1 +unc-119(+)]* hermaphrodites (n=30) produced oocytes and sperm and were self-fertile. This result established that the P222L mutation in SACY-1 causes the Mog phenotype.

The suppression of *fog-2* sterility by reduction-of-function *sacy-1* mutations is consistent with *sacy-1(+)* possessing a function that promotes the oocyte fate; this function is non-essential, however, because the strongest loss-of-function *sacy-1* alleles are able to produce oocytes, which nevertheless undergo necrotic degeneration. Thus, the *sacy-1(tn1481)* Mog phenotype suggests this mutant allele, although recessive, possesses an activity antagonistic to this oocyte-promoting function in the sperm-to-oocyte switch. To genetically characterize *sacy-1(tn1481)* further, we analyzed the phenotype of *sacy-1(tn1481)/sacy-1(tm5503* null*)* heterozygotes. Whereas all *sacy-1(tn1481)* homozygotes (n=50) displayed a Mog phenotype, all *sacy-1(tn1481)/sacy-1(tm5503)* heterozygotes (n=48) produced both oocytes and sperm and were self fertile. This result suggests that the *sacy-1(tn1481)* Mog phenotype is

dosage sensitive and that the mutant allele appears to be a recessive gain-of-function mutation that might antagonize proteins that normally function with SACY-1, likely other components of the spliceosome as discussed below.

In *C. elegans*, a genetic hierarchy controls germline sex determination (Figure 3). The failure of *sacy-1(RNAi)* to suppress the sterility of the dominant strongly feminizing *tra-2(e2020)* mutation, which deletes GLD-1 binding sites within the *tra-2 3'-UTR*, was interpreted in the context of a model in which *sacy-1(+)* promotes the oocyte fate in opposition to *fog-2* and *gld-1* at the level of *tra-2* (Figure 3; Kim *et al*. 2012). Because the evaluation of potential interactions between *sacy-1* and *tra-2* relied on *sacy-1(RNAi)*, there was the concern that this treatment reduced but did not eliminate the function of *sacy-1*. Thus, we reevaluated the interaction between *tra-2* and *sacy-1* genetically. In the first approach, we combined the *sacy-1(tm5503)* null allele with *tra-2(e2020)*. We analyzed the sexual fate of the germline by staining dissected gonads from adult animals with oocyte (RME-2) and sperm (MSP) markers. Whereas all wild-type gonad arms examined (n=30) expressed RME-2 and MSP, all gonad arms of *sacy-1(tm5503)*; *tra-2(e2020)* animals (n=26) expressed only RME-2 and not MSP (Figure 4). This result is consistent with the model in which *sacy-1* promotes the oocyte fate by promoting the function of *tra-2*. Although the germlines of *sacy-1(tm5503)*; *tra-2(e2020)* adults were feminized, oocytes underwent meiotic maturation constitutively, consistent with the finding that *sacy-1* is a negative regulator of meiotic maturation (Kim *et al*. 2012). *sacy-1(tm5503)*; *tra-2(e2020)* animals did however exhibit a highly penetrant ovulation defect, which caused endomitotic oocytes to accumulate in the gonad arm (Emo phenotype; Figure 4).

To extend these observations, we examined germline sexual fates in dissected gonads from *sacy-1(tn1481*Mog*); tra-2(e2020)* adults. Whereas all wild-type gonad arms examined (n=21) expressed MSP and contained sperm, none of the *sacy-1(tn1481Mog); tra-2(e2020)* gonad arms (n=37) expressed MSP or contained sperm. We noted that the Emo phenotype was less penetrant in *sacy-1(tn1481Mog); tra-2(e2020)* gonad arms (46% penetrance). These results are consistent with the

548 possibility that *sacy-1(+)* promotes the oocyte fate by promoting the function of *tra-2* in the germline
549 and suggests that *sacy-1(tn1481*Mog*)* may interfere with this function.

550 Interestingly, recessive loss-of-function mutations in six genes, *mog-1–6*, cause a Mog
551 phenotype and encode spliceosomal components (Graham and Kimble 1993; Graham *et al*. 1993; Puoti
552 and Kimble 1999, 2000; Belfiore *et al*. 2004; Zanetti *et al*. 2011). Mutation and RNAi depletion of
553 many splicing factors have been observed to result in a Mog phenotype, suggesting that the germline
554 sex determination process is particularly sensitive to disruptions in RNA splicing (Mantina *et al*. 2009;
555 Kerins *et al*. 2010; Wang *et al*. 2012; Novak *et al*. 2015). Prior studies focusing on the *C. elegans* soma
556 were interpreted in the context of a model in which *mog-1–mog-6* might function at the level of *fem-3*
557 through 3'UTR-dependent translational regulation (Gallegos *et al*. 1998; Figure 3); however, the
558 experiments in that study did not address the regulation of *fem-3* in the germline. We previously
559 showed that *sacy-1(tm5503); fem-3(e1996)* adult XX animals had feminized germlines (Kim *et al*.
560 2012). To examine the genetic relationship between *sacy-1* and *fem-3* further, we generated *sacy-*
561 *1(tn1481Mog); fem-3(e1996)* double mutants. We observed that 92% (n=23) of *sacy-1(tn1481Mog);*
562 *fem-3(e1996)* animals were feminized. Mating of *sacy-1(tn1481Mog); fem-3(e1996)* females (n=29) to
563 wild-type males resulted in the production of embryos that failed to hatch (n=4140, 99.8%) or arrested
564 as larvae (n=7, 0.2%). This result indicates that two copies of *sacy-1(tn1481)* in the maternal germline,
565 but not one [e.g., *sacy-1(tn1481)/sacy-1(tm5503)* heterozygotes are fertile] are incompatible with
566 embryonic development. We found that 8% (n=2) of *sacy-1(tn1481*Mog*); fem-3(e1996)* animals
567 (n=25) produced oocytes and sperm and a few dead embryos (one of these animals produced sperm in
568 one gonad arm but not the other). This result suggests that the *sacy-1(tn1481)* mutation can promote
569 sperm development independent of zygotic *fem-3(+)* activity, consistent the genetic epistasis pathway
570 (Figure 3; Zanetti and Puoti 2013). We did observe that a reduction in *fem-3* dosage could suppress the
571 *sacy-1(tn1481)* Mog phenotype (n=60). Specifically, whereas 65% (n=39) of *sacy-1(tn1481); fem-*
572 *3(e1996)*/+ animals were Mog, exclusively producing sperm, 33% (n=20) produced sperm and

oocytes, and one animal (2%) was feminized. Since SACY-1 genetically and biochemically interacts with components of the spliceosome, we suggest that the *sacy-1(tn1481)* mutation antagonizes functions of the spliceosome needed for germline sex determination and oogenesis.

The gain-of-function sacy-1(tn1480) allele confers multiple pleiotropic phenotypes in a temperature-dependent manner: Interestingly, *sacy-1(tn1480)* displayed both cold-sensitive (15°C) and temperature-sensitive (25°C) defects. At 15°C, *sacy-1(tn1480)* homozygotes (n=55), which were the offspring of heterozygous parents grown at 15°C, laid dead eggs and produced arrested larvae (91%) or produced very few progeny (9%). At 25°C, *sacy-1(tn1480)* hermaphrodites were sterile and produced abnormal and fertilization-defective sperm (Figure 5). *sacy-1(tn1480)* hermaphrodite sterility is rescued by mating with wild-type males at 25°C. In addition to producing oocytes, some *sacy-1(tn1480)* adult hermaphrodites continued to produce sperm, as swollen germ cells specified in the male fate were detected distal to the loop region in 42% of gonad arms examined (Figure 5; n=12). Thus, in addition to the other phenotypes it confers, the *sacy-1(tn1480)* mutation perturbs the sperm-to-oocyte switch at 25°C. We also observed that *sacy-1(tn1480)* conferred a dominant high-incidence of males (Him) phenotype; *sacy-1(tn1480)/+* heterozygous hermaphrodites produced 1.6% male progeny (n=3759), as compared to 0.1% for the wild-type control (n=6044; $p<0.01$, Fisher's exact test). Genetic mapping showed that the temperature-dependent pleiotropic defects were inseparable from the *sacy-1(tn1480)* mutation (see Materials and Methods). Like *sacy-1(tn1481)*, the defects conferred by *sacy-1(tn1480)* were dosage sensitive. At 25°C, nearly all *sacy-1(tn1480)/sacy-1(tm5503)* heterozygotes (99%, n=88) were fertile (the average brood size was 132 ± 64, n=34); however, the majority of *sacy-1(tm5503)* homozygotes (85.3%, n=231) they produced burst as adults (Table 6). This result suggests that maternal *sacy-1(tn1480)* activity can antagonize the spliceosome in the absence of zygotic *sacy-1(+)* function. By these genetic criteria, *sacy-1(tn1480)* exhibits recessive and weakly dominant gain-of-function properties, depending on the phenotype examined.

The oncogenic DDX41 R525H mutation confers weak antagonistic activity in C. elegans

The R525H mutation in DDX41 has been reported in myeloid leukemias both as newly arising somatic mutations specific to the neoplastic cells, as well as inherited germline mutations (Polprasert *et al*. 2015; Lewinsohn *et al*. 2016; Sébert *et al*. 2019). Thus, it was of interest to examine the impact of the analogous mutation (R534H) on *sacy-1* function. Interestingly, a substitution at the adjacent amino acid (G533R) results in the *sacy-1(tn1385)* reduction-of-function mutation (Figure 1). Thus, we used genome editing to introduce the R534H mutation in the *C. elegans* genome (see Materials and Methods). By several criteria, *sacy-1(tn1887*[R534H]*)* homozygotes were indistinguishable from the wild type. Neither did *sacy-1(tn1887)* suppress *acy-4* sterility (n=140; *sacy-1(tn1887); acy-4(ok1806)* brood size was 1.5 ± 2.3) nor did it suppress *fog-2* sterility (n=48). All unmated *sacy-1(tn1887); fog-2(oz40)* gonad arms examined (n=96) exhibited stacked oocytes, which indicates that the *sacy-1(tn1887)* mutation does not derepress meiotic maturation in the absence of sperm, like strong reduction-of-function mutations do. Further, the *sacy-1(tn1887*[R534H]*)* did not enhance the Tumorous phenotype of a gain-of-function *glp-1/Notch* allele (Table 4). The brood size of *sacy-1(tn1887)* (204 ± 37; n=20) at 25°C was indistinguishable from that of the wild type (202 ± 62, n=30; p>0.8, two-sample Z-test). Also, the incidence of males (0.2%, n=4087) was similar to that observed in the wild type (0.1%, n= 6044). When placed in trans to the *sacy-1(tm5503)* null mutation, *sacy-1(tn1887)/sacy-1(tm5503)* heterozygotes were found to be fertile at all temperatures examined (15°, 20°, and 25°C (n=104)). However, we did observe that *sacy-1(tn1887)* significantly enhanced the dominant Him phenotype of *sacy-1(tn1480)* ($p<0.05$, Fisher's exact test); *sacy-1(tn1887)/sacy-1(tn1480)* heterozygotes produced 5.7% males at 25°C (n=1483) as compared to 1.6% for the *+/sacy-1(tn1480)* control (n=3759). The brood size of *sacy-1(tn1887)/sacy-1(tn1480)* heterozygotes at 25°C (74 ± 65, n=20) was also significantly lower than that of the *+/sacy-1(tn1480)* control (188 ± 68, n=20; $p<0.001$, two-sample Z-test). Because, *sacy-1(tn1480)/sacy-1(tm5503)* heterozygotes do not exhibit an

enhanced Him phenotype at 25°C (0.7% males, n=4493), the *sacy-1(tn1887*[R534H]*)* mutation appears to possess a weak antagonistic activity.

Impact of sacy-1 on the transcriptome

Depletion of SACY-1 using the auxin-inducible degradation system: RNA sequencing studies using human patient samples suggested a role for DDX41 in splice site selection for a small number of human genes (Polprasert *et al*. 2015). Thus, we sought to address the impact of SACY-1 on the transcriptome by exploiting the power of the *C. elegans* system for transcriptomics under genotypically and experimentally well-controlled conditions. We chose to use the auxin-inducible degradation system (Zhang *et al.* 2015) to acutely deplete SACY-1 in the adult stage and thus avoid indirect impacts on the transcriptome arising as a developmental consequence of strong loss-of-function phenotypes (e.g., germline degeneration and cell fate changes). Because the genetic analysis established requirements for *sacy-1(+)* function in both the germline and soma, we used strains bearing germline (CA1352 *ieSi64*) or somatically expressed (CA1200 *ieSi57*) TIR1 F-box proteins to deplete AID::GFP::SACY-1 in each tissue individually (Figure S5 and Figure S6). Depletion of AID::GFP::SACY-1 in the germline starting at approximately the L3 stage phenocopied the gamete degeneration phenotype in a small proportion of the animals (3 of 270; Figure S5). This result is consistent with genetic mosaic analysis showing that the gamete degeneration phenotype is cell autonomous (Kim *et al*. 2012), and it also highlights the difficulty of recapitulating null phenotypes through auxin-inducible degradation. When AID::GFP::SACY-1 is depleted in the germline starting at the L4 stage, many of their F1 progeny arrest as embryos or larvae, consistent with the idea that maternally contributed *sacy-1(+)* activity is essential. Animals that escape the lethality and progress to adulthood often display the germline degeneration phenotype (40%; n=139). To deplete AID::GFP::SACY-1 in the soma, we placed L4 larvae on media containing 2 mM auxin. The resulting F1 progeny grew very slowly, taking approximately 4–6 days to reach adulthood (instead of 2.5 days)

and were sterile (Figure S5). Taken together, depletion of SACY-1 using the auxin-inducible degradation system resulted in a reduction-of-function condition less severe than the null phenotype but more severe than conferred by the reduction-of-function missense alleles (Table 5).

For analysis of transcriptomes, we grew adult hermaphrodites to the young adult stage on normal growth media and then transferred them to media containing 2 mM auxin for 24 hours before preparing total RNA for RNA sequencing. Examination of the worms showed that AID::GFP::SACY-1 was depleted from the targeted tissues (Figure S6). Total RNA was prepared from each of three biological replicates and their respective controls, which were the parent strains expressing TIR1 in the germline (*ieSi64*) or soma (*ieSi57*) also treated with auxin. Poly(A+) mRNA was sequenced using 150 bp paired-end reads and the sequencing reads were aligned to the genome. Principal component analysis (PCA) revealed that the biological replicates clustered together (Figure 6A), which is indicative of experimental reproducibility. However, PCA indicated that the control strains for the germline (CA1352) and soma (CA1200) depleted samples did not cluster together, which indicates that under these conditions the two strain backgrounds exhibit marked differences in their transcriptomes (Figure 6A), a finding that was further confirmed with a more granular assessment of mRNA expression level differences of individual genes (Figure S7A). Thus, in our analysis we compared the germline- and soma-depleted SACY-1 transcriptomes only to their respective controls.

Changes in transcript abundance following SACY-1 depletion: We observed two classes of transcriptome alterations upon depletion of SACY-1 in the germline or soma: changes in transcript abundance and alterations in splicing patterns. In terms of transcript abundance, we observed 242 down-regulated genes (two-fold down-regulation, adjusted $p<0.05$, FPKM in soma control ≥ 2.5, mean counts across samples > 25) in the RNA samples depleted for somatic SACY-1 (Figure 6, B and C; File S2). Notably these down-regulated genes included many cuticle collagen genes and genes affecting cuticular morphology and body size (*col-17*, *col-41*, *col-46*, *col-47*, *col-90*, *col-128*, *col-149*,

672 *dpy-3*, *dpy-4*, *dpy-5*, *dpy-6*, *dpy-8*, *dpy-9*, *dpy-13*, *dpy-20*, *lon-3*, *mlt-7*, *qua-1*, *rol-6*, *rol-8*, *sqt-1*, and
673 *sqt-2*). Consistent with this observation, the top enriched gene ontology (GO) term for transcripts
674 reduced in abundance in the SACY-1 soma-depleted samples was "cuticle development involved in
675 collagen and cuticulin-based cuticle molting cycle" (Figure S7B). We also observed 242 up-regulated
676 genes (two-fold up-regulation, adjusted $p<0.05$, FPKM in SACY-1 soma-deplete ≥ 2.5, mean counts
677 across samples > 25) in the SACY-1 soma-depleted samples (Figure 6, B and C; File S2). The top
678 enriched GO term for transcripts with increased abundance in the SACY-1 soma-depleted samples
679 related to cellular responses to heat stress, the unfolded protein response, and innate immune responses
680 (Figure S7), suggesting that the organism might perceive the reduction of *sacy-1(+)* function as a
681 stressor and might then mount a response that then alters the transcriptome.
682 In the SACY-1 germline-depleted samples, we observed 126 down-regulated genes (two-fold
683 down-regulation, adjusted $p<0.05$, FPKM in germline control ≥ 2.5, mean counts across samples > 25;
684 Figure 6, B and D; File S2). The top enriched GO terms for transcripts with decreased abundance in
685 the SACY-1 germline-depleted samples included the response to heat stress and the unfolded protein
686 response (Figure S7B), suggesting the response to *sacy-1(+)* depletion differs between the soma and
687 germline. Among the 311 transcripts increased in abundance in the SACY-1 germline-depleted sample
688 was *her-1* (two-fold up-regulation, adjusted $p<0.05$, FPKM in SACY-1 germline-deplete ≥ 2.5, mean
689 counts across samples > 25; Figure 6, B, D, and E; File S2). This might be due to an increase in X
690 chromosome non-disjunction in embryos located in the uterus following germline depletion of *sacy-*
691 *1(+)*, but this possibility was not investigated. Because *her-1* likely encodes an inhibitory ligand for
692 the TRA-2 receptor in the sex-determination pathway (Perry *et al*. 1993; Figure 3), we tested whether
693 the *her-1(hv1y101)* null mutation could suppress the Mog phenotype of the recessive gain-of-function
694 *sacy-1(tn1481)* mutation, but this proved not to be the case (n=53 gonad arms). Since the genetic
695 epistasis results suggest that SACY-1 promotes the expression of TRA-2 (Figure 3), we examined the
696 effect of SACY-1 depletion in the germline on the levels of *tra-2* mRNA and the fidelity of its

splicing. We observed no statistically significant change in *tra-2* mRNA levels or its splicing patterns (Figure 6F). We did not examine the expression of TRA-2 protein after SACY-1 depletion because a recent study suggested that TRA-2 protein expression in the wild-type germline is below the immunofluorescence detection limit of immunofluorescence (Hu *et al*. 2019).

Alteration of splicing patterns following SACY-1 depletion: In the SACY-1 soma-depleted samples, we observed significant (FDR<0.05) alterations in splicing patterns for 1606 transcripts (Figure 7A). These splicing alterations fell into several broad classes: the use of alternative 5' splice sites, the use of alternative 3'splice sites, abnormal splicing within an exon, skipped exons, and retained introns. The largest class of splicing changes was the use of alternative 3' splice sites, consistent with the fact that DDX41 was shown to be recruited to the C complex, which mediates the second step in splicing (Bessonov *et al.* 2008). Multiple splicing defects were sometimes observed within a single gene. For example, in the case of the RNA-binding protein ETR-1, which has multiple isoforms and is expressed in the soma and germline (Boateng *et al*. 2017), depletion of SACY-1 results in intron retention and multiple alterations in 3'-splice-site usage (Figure 7B). In the SACY-1 germline-depleted samples we observed significant (FDR<0.05) alterations in splicing for 796 transcripts (Figure 7A). Thus, splicing defects appeared less prevalent in the SACY-1 germline-depleted samples than the SACY-1 soma-depleted samples. One possibility is that nonsense mediated decay or other surveillance pathways actively clear misspliced mRNAs from the germline. Some alternative splicing events were observed in both the RNA preparations depleted for SACY-1 in the germline and the soma (Figure 7A). For example, we observed retention of an intron in *prdx-6* mRNA in both experiments (Figure 7C). Likewise, we observed alternative 3' splice site selection for the heterochronic gene *lin-28* in both SACY-1-depleted samples (Figure 7D).

Germline sex-specific splicing patterns and the involvement of SACY-1: As we analyzed the changes in splicing patterns following SACY-1, we noticed changes in alternative splicing patterns that appeared to correlate with the sex of the germline. To investigate this observation more fully, we reanalyzed the data of Ortiz *et al*. (2014), who reported the transcriptomes of genotypically XX animals exclusively undergoing oogenesis or spermatogenesis as a consequence of containing a loss-of-function *fog-2* mutation or a gain-of-function *fem-3* mutation, respectively. This dataset was previously used to identify alternative isoform usage in the germline (Oritz *et al*. 2014). In analyzing their dataset for alternative splicing events, we observed 1600 genes for which there was a significant (FDR<0.05) germline sex-specific splicing pattern (Figure S8; File S3). We noted that upon SACY-1 depletion in either the soma or germline, oocyte-enriched splicing events were favored (Figure 7A and Figure S8). This result suggests that SACY-1 plays a role in the selection of 3' splice sites for many genes and raises the possibility that the appropriate balance of "spliceoforms" may be play a role in cellular differentiation.

DISCUSSION

In this study, we report the results of a molecular genetic and biochemical analysis of SACY-1/DDX41 in *C. elegans*, conducted to gain potential insights into how *DDX41* mutations might contribute to MDS and AML in humans. DDX41 is a component of the spliceosomal C complex (Jurica *et al*. 2002; Bessonov *et al*. 2008), which carries out the second step in splicing. Pre-mRNA splicing is an essential process in eukaryotes (reviewed by Wahl *et al*. 2009). Thus, the finding that mutations in highly conserved genes encoding spliceosomal components are frequently found in hematological malignancies was unexpected (reviewed by Yoshida and Ogawa 2014). Unfortunately, the genetic properties of disease-causing mutations in spliceosomal proteins have been difficult to assess. Nonetheless, the observation that many of these missense mutations map to highly conserved amino acids, within biochemically defined structural and functional domains, might suggest that they reduce but not eliminate gene function. An alternative possibility is that some of the oncogenic missense mutations might confer antagonistic gain-of-function properties. Indeed, oncogenic mutations in several splicing factors (e.g., SF3B1, U2AF1, SRSDF2, and SRSR2) present in the heterozygous condition (Yoshida and Ogaawa 2014); however, it is probable that newly arising mutations in hematopoetic lineages, in combination with the germline mutations, contribute to neoplastic development.

In this regard, the *DDX41* mutations inherited and arising in familial cases of AML are particularly informative (Polprasert *et al*. 2015). Affected individuals often inherit one copy containing a mutation, which is likely to be a null mutation (e.g., a frameshift mutation, pD140fs). In addition to this *DDX41* germline mutation, the neoplasms in these patients invariably contain a second copy with a somatic mutation that arose in the hematopoietic lineage. Several specific *DDX41* somatic mutations (e.g., R525H) arise independently with high prevalence, suggesting that they markedly contribute to neoplastic development. These somatic *DDX41* mutations are invariably missense mutations affecting conserved amino acids but have never been found to include candidate null alleles (e.g., frameshift

mutations or premature termination codons). Thus, these somatically arising mutations are unlikely to eliminate DDX41 function. The presumption is that biallelic mutations disrupting DDX41 function might be lethal. In line with this view, a recent report found that two related patients with biallelic DDX41 missense mutations exhibited a more severe syndrome characterized by dysmorphic skeletal and facial features, psychomotor delays, intellectual disability, and early onset leukemia (Diness *et al*. 2018).

Here we build upon our prior work (Kim *et al*. 2012) to conduct a comprehensive molecular genetic analysis of SACY-1/DDX41 function in *C. elegans*. Recent work of others has used the *C. elegans* system to gain information on oncogenic mutations in the SF3B1 spliceosomal protein (Serrat *et al*. 2019). Our results reveal that *sacy-1* mutations confer a range of phenotypes, from highly pleiotropic defects affecting the germline and soma to very specific defects affecting cell differentiation and cell cycle regulation. Reduction-of-function *sacy-1* alleles are homozygous viable and fertile, yet affect germline sex determination and the regulation of oocyte meiotic maturation (Kim *et al*. 2012; this work). Animals homozygous for *sacy-1* null mutations grow to adulthood but exhibit a gamete degeneration phenotype and are sterile. Feminization of the germline delays oocyte degeneration, which enables *sacy-1* null mutant females to be mated and produce embryos. However, these embryos invariably die, revealing an essential maternal requirement for development. Maternally provided *sacy-1(+)* must in turn be sufficient for homozygous *sacy-1* null mutant animals (produced from heterozygous parents) to grow to adulthood.

Several *sacy-1* mutant alleles exhibit genetic properties that suggest they can counteract *sacy-1(+)* function, potentially by compromising the function of the spliceosome. Most notable among these mutations is *sacy-1(tn1481)*, which confers a masculinization of the germline phenotype resulting from the overproduction of sperm to the exclusion of the oocyte fate. Since multiple reduction-of-function *sacy-1* alleles suppress the feminization of the germline phenotype caused by null mutations in *fog-2* (Kim *et al*. 2012; this work), *sacy-1(+)* must possess a function to promote the oocyte fate. This

oocyte-promoting function of *sacy-1(+)* might not be essential because *sacy-1* null mutants produce oocytes, which nonetheless undergo necrotic degeneration. The caveat here is that *sacy-1* null mutants only develop to adulthood because of maternally provided *sacy-1(+)*, which might be sufficient to promote oogenesis. In any case, the *sacy-1(tn1481)* mutation might disrupt an oocyte-promoting function either by interfering with maternally provided SACY-1 activity or proteins with which it associates.

Several observations are consistent with the possibility that *sacy-1(tn1481)* interferes with or compromises the function of the spliceosome in germline sex determination in a dosage-sensitive manner. This view is also supported by our tandem affinity purification results showing that SACY-1 is a component of the *C. elegans* spliceosome and genetically interacts with spliceosomal components. Significantly, multiple *C. elegans* spliceosomal components, functioning at different steps of the splicing reaction, can mutate to a masculinization of germline phenotype (reviewed by Zanetti and Puoti 2013). Interestingly, when placed in trans to a *sacy-1* null mutation (e.g., *tm5503*), the resulting *sacy-1(tn1481)/sacy-1(tm5503)* heterozygous animals are viable and fertile and can be maintained indefinitely as a heterozygous strain. This highly informative genetic result suggests that a single dose of *sacy-1(tn1481)* can mediate all its essential functions, but that two doses of the mutant protein interferes with the normal mechanisms of germline sex determination (i.e., *sacy-1(tn1481)* is a recessive gain-of-function antimorphic mutation). Although *sacy-1(tn1481)/sacy-1(tm5503)* heterozygous adult hermaphrodites are fertile, when *sacy-1(tn1481); fem-3(e1996)* females are mated to wild-type males, they produce embryos that invariably fail to hatch. Similar results are obtained with the six other *mog* genes (Graham and Kimble 1993; Graham *et al*. 1993), which encode spliceosomal proteins (Puoti and Kimble 1999; Puoti and Kimble 2000; Belfiore *et al.* 2004; Kasturi *et al*. 2010; Zanetti *et al*. 2011). Interestingly the P222L amino acid substitution found in *sacy-1(tn1481)* is adjacent to the Q motif, which participates in nucleotide binding and hydrolysis (Schütz *et al.* 2010). It is tempting to speculate that SACY-1/DDX41 might promote remodeling of spliceosomes during the

splicing reaction and that two doses of SACY-1 P222L might disrupt these rearrangements. In a similar vein, *sacy-1(tn1479*[G504E]*)* exhibits a phenotype more severe than a null allele, suggesting that this mutation in the helicase domain too might possess a dosage-sensitive antimorphic activity. Whether missense alleles in human DDX41 also possess antimorphic activity will require additional work, including biochemical analyses.

We imported the oncogenic *DDX41*[R525H] mutation into *C. elegans* using CRISPR-Cas9 genome editing (R534H in SACY-1). Our analysis revealed that in *C. elegans*, this mutation possesses very weak antagonistic activity. While it is possible that the genetic properties of this mutation might differ between *C. elegans* and mammalian systems, it is worthwhile noting that the oncogenic variant must support the high levels of proliferation characteristic of neoplastic cells. While all the *sacy-1* mutations we isolated in forward genetic screens occur at conserved amino acids, none of them match the oncogenic mutations thus far isolated (Polprasert *et al*. 2015; Cardoso *et al*. 2016; Lewinsohn *et al*. 2016; Li *et al*. 2016; Diness *et al*. 2018 ; Sébert *et al*. 2019). This observation is consistent with the idea that the oncogenic mutations are at most weakly antagonizing or weak reduction-of-function mutations, and thus would not have been isolated in forward genetic screens that require a substantial reduction in function.

An attractive idea is that oncogenic mutations affecting the spliceosome contribute to neoplastic development through effects on gene expression occurring through alterations in RNA splicing, as well as effects on the transcriptional machinery or RNA stability (Yoshimi *et al*. 2019). Consistent with this idea, RNAi depletion of the *C. elegans* spliceosomal protein RSR-2 affects transcript levels without major impacts on splicing (Fontrodona *et al*. 2013). In this study, we examined the effects of SACY-1 depletion at the adult stage on the transcriptome. In the soma and the germline, we observed splicing-independent impacts on the abundance of many transcripts. The gene expression changes observed suggest that depletion of SACY-1 might elicit a stress response. If analogous processes occur after perturbations of the spliceosome in humans, such stress responses

might contribute to oncogenesis and could represent therapeutic targets. In *C. elegans*, we observed instances of missplicing following SACY-1 depletion, though missplicing events more prevalent when SACY-1 was depleted from the soma as compared to the germline. The extent to which gene expression changes and splicing alterations contribute to the various *sacy-1* mutant phenotypes will require further study but will likely provide insights relevant to spliceosomal perturbations in humans.

ACKNOWLEDGMENTS

This paper is dedicated to the memory of Michael A. Miller, our colleague and friend whose scientific contributions will not be forgotten. We thank Donna Coetzee for technical assistance. We are grateful to Joshua Arribere, Daniel Dickinson, Barth Grant, Tim Schedl, and Jordan Ward for providing strains or reagents. Some strains were provided by the Caenorhabditis Genetics Center, which is funded by grant P40OD010440 from the NIH Office of Research Infrastructure Programs. We thank Gabriela Huelgas-Morales, Zohar Sachs, and Todd Starich for their helpful suggestions for the manuscript. This work was supported by NIH grant GM57173 to D.G.

LITERATURE CITED

Agarwal, A., D. Koppstein, J. Rozowsky, A. Sboner, L. Habegger *et al*., 2010 Comparison and calibration of transcriptome data from RNA-Seq and tiling arrays. BMC Genomics 11: 383.

Arribere, J. A., R. T. Bell, B. X. Fu, K. L. Artiles, P. S. Hartman *et al*., 2014 Efficient marker-free recovery of custom genetic modifications with CRISPR/Cas9 in *Caenorhabditis elegans*. Genetics 198: 837–846.

Belfiore, M., P. Pugnale, Z. Saudan, and A. Puoti, 2004 Roles of the *C. elegans* cyclophilin-like protein MOG-6 in MEP-1 binding and germline fates. Development 131: 2935–2945.

Bertram, K., D. E. Agafonov, W.-T. Liu, O. Dybkov, C. L. Will *et al*., 2017 Cro-EM structure of a human spliceosome activated for step 2 of splicing. Nature 542: 318–323.

Bessonov, S., M. Anokhina, A. Krasauskas, M. M. Golas, B. Sander *et al*., 2010 Characterization of purified human B^{act} spliceosomal complexes reveals compositional and morphological changes during spliceosome activation and first step catalysis. RNA 16: 2384–2403.

Bessonov, S., M. Anokhina, C. L. Will, H. Urlaub, and R. Lührmann, 2008 Isolation of an active step I spliceosome and composition of its RNP core. Nature 452: 846–850.

Boateng, R., K. C. Q. Nguyen, D. H. Hall, A. Golden, and A. K. Allen, 2017 Novel functions for the RNA-binding protein ETR-1 in *Caenorhabditis elegans* reproduction and engulfment of germline apoptotic corpses. Dev. Biol. 429: 306–320.

Cardoso, S. R., G. Ryan, A. J. Walne, A. Ellison, R. Lowe *et al.*, 2016 Germline heterozygous *DDX41* variants in a subset of familial myelodysplasia and acute myeloid leukemia. Leukemia 30: 2083–2086.

Chaudhary, N., C. McMahon, and G. Blobel, 1991 Primary structure of a human arginine-rich nuclear protein that colocalizes with spliceosome components. Proc. Natl. Acad. Sci. USA 88: 8189–8193.

Coltri, P. P., M. G. P. dos Santos, and G. H. G. da Silva, 2019 Splicing and cancer: challenges and

opportunities. WIREs RNA 10: e1527.

De, I., S. Bessonov, R. Hofele, K. dos Santos, C. L. Will *et al*., 2015 The RNA helicase Aquarius exhibits structural adaptations mediating its recruitment to spliceosomes. Nat. Struct. Mol. Biol. 22: 138–144.

Dejima, K., S. Hori, S. Iwata, Y. Suehiro, S. Yoshina *et al*., 2018 An aneuploidy-free and structurally defined balancer chromosome toolkit for *Caenorhabditis elegans*. Cell Rep. 22: 232–241.

DeNicola, A. B., and Y. Tang, 2019 Therapeutic approaches to treat human spliceosomal diseases. Curr. Opin. Biotechnol. 60: 72–81.

Dickinson, D. J., J. D. Ward, D. J. Reiner, and B. Goldstein, 2013 Engineering the *Caenorhabditis elegans* genome using Cas9-triggered homologous recombination. Nat. Methods 10: 1028–1034.

Diness, B. R., L. Risom, T. L. Frandsen, B. Hansen, M. K. Andersen *et al.*, 2018 Putative new childhood leukemia cancer predisposition syndrome caused by germline bi-allelic missense mutations in *DDX41*. Genes Chromosomes Cancer 57: 670–674.

Ding, L., T. J. Ley, D. E. Larson, C. A. Miller, D. C. Koboldt, *et al.*, 2012 Clonal evolution in relapsed acute myeloid leukaemia revealed by whole-genome sequencing. Nature 481: 506-510.

Effenberger, K. A., V. K. Urabe, and M. S. Jurica, 2017 Modulating splicing with small molecular inhibitors of the spliceosome. WIREs RNA 8: e1381.

Fabrizio, P., J. Dannenberg, P. Dube, B. Kastner, H. Stark *et al*., 2009 The evolutionarily conserved core design of the catalytic activation step of the yeast spliceosome. Mol. Cell 36: 593–608.

Fica, S. M., C. Oubridge, M. E. Wilkinson, A. J. Newman, and K. Nagai, 2019 A human postcatalytic spliceosome structure reveals essential roles of metazoan factors for exon ligation. Science 363: 710–714.

Fontrodona, L., M. Porta-de-la-Riva, T. Morán, W. Niu, M. Díaz *et al*., 2013 RSR-2, the *Caenorhabditis elegans* ortholog of human spliceosomal component SRm300/SRRM2,

regulates development by influencing the transcriptional machinery. PloS Genetics 9: e1003543.

Francis, R., E. Maine, and T. Schedl, 1995a Analysis of the multiple roles of *gld-1* in germline development: interactions with the sex determination cascade and the *glp-1* signaling pathway. Genetics 139: 607–630.

Francis, R., M. K. Barton, J. Kimble, and T. Schedl, 1995b *gld-1*, a tumor suppressor gene required for oocyte development in *Caenorhabditis eleg*ans. Genetics 139: 579–606.

Gallegos, M., J. Ahringer, S. Crittenden, and J. Kimble, 1998 Repression by the 3' UTR of *fem-3*, a sex-determining gene, relies on a ubiquitous *mog*-dependent control in *Caenorhabditis elegans*. EMBO J. 17: 6337–6347.

Govindan, J. A., H. Cheng, J. E. Harris, and D. Greenstein, 2006 $G\alpha_{o/i}$ and $G\alpha_s$ signaling function in parallel with the MSP/Eph receptor to control meiotic diapause in *C. elegans*. Curr. Biol. 16: 1257–1268.

Govindan, J. A., S. Nadarajan, S. Kim, T. A. Starich, and D. Greenstein, 2009 Somatic cAMP signaling regulates MSP-dependent oocyte growth and meiotic maturation in *C. elegans*. Development 136: 2211–2221.

Graham, P. L., and J. Kimble, 1993 The *mog-1* gene is required for the switch from spermatogenesis to oogenesis in *Caenorhabditis elegans*. Genetics 133: 919–931.

Graham, P. L., T. Schedl, and J. Kimble, 1993 More *mog* genes that influence the switch from spermatogenesis to oogenesis in *Caenorhabditis elegans*. Dev. Genet. 14: 471–484.

Grant, B., and D. Hirsh, 1999 Receptor-mediated endocytosis in the *Caenorhabditis elegans* oocyte. Mol. Biol. Cell 10**:** 4311-4326.

Grainger, R. J., and J. D. Beggs, 2005 Prp8 protein: at the heart of the spliceosome. RNA 11: 533–557.

Grinfeld, J., J. Nangalia, E. J. Baxter, D. C. Wedge, N. Angelopoulos *et al.*, 2018 Classification and personalized prognosis in myeloproliferative neoplasms. N. Engl. J. Med. 379: 1416–1430.

Harris, T. W., J. Baran, T. Bieri, A. Cabunoc, J. Chan *et al*., 2013 WormBase 2014: new views of curated biology. Nucleic Acids Res. 42: D789–D793.

Haselbach, D., I. Komarov, D. E. Agafonov, K. Hartmuth, B. Graf *et al*., 2018 Structure and conformational dynamics of the human spliceosomal B^{act} complex. Cell 172: 454–464.

Hastings, M. L., E. Allemand, D. M. Duelli, M. P. Myers, and A R. Krainer, 2007 Control of pre-mRNA splicing by general splicing factors PUF60 and $U2AF^{65}$. PLoS One 2: e538.

Henn, A., M. J. Bradley, and E. M. De La Cruz, 2012 ATP utilization and RNA conformational rearrangement by DEAD-box proteins. Annu. Rev. Biophys. 41: 247–267.

Herold, N., C. L. Wil, E. Wolf, B. Kastner, H. Urlaub *et al*., 2009 Conservation of the protein composition and electron microscopy structure of *Drosophila melanogaster* and human spliceosomal complexes. Mol. Cell. Biol. 29: 281–301.

Hu, S., L. E. Skelly, E. Kaymak, L. Freeberg, T.-W. Lo *et al*., 2019 Multi-modal regulation of *C. elegans* hermaphrodite spermatogenesis by the GLD-1-FOG-2 complex. Dev. Biol. 446: 193–205.

Irion, U., M. Leptin, K. Siller, S. Fuerstenberg, Y. Cai *et al.*, 2004 Abstrakt, a DEAD box protein, regulates Insc levels and asymmetric division of neural and mesodermal progenitors. Current Biology 14: 138–144.

Jiang, Y., Y. Zhu, Z.-J. Liu, and S. Ouyang, 2017 The emerging roles of the DDX41 protein in immunity and diseases. Protein Cell 8: 83–89.

Jiao, A. L., R. Perales, N. T. Umbreit, J. R. Haswell, M. E. Piper *et al*., 2019 Human nuclear RNAi-defective 2 (NRDE2) is an essential RNA splicing factor. RNA 25: 352–3463.

Jones, A. R., and T. Schedl, 1995 Mutations in *gld-1*, a female germ cell-specific tumor suppressor gene in *Caenorhabditis elegans*, affects a conserved domain also found in Src-associated protein Sam68. Genes Dev. 9: 1491–1504.

Jurica, M. S., L. J. Licklider, S. P. Gygi, N. Grigorieff, and M. J. Moore, 2002 Purification and

characterization of native spliceosomes suitable for three-dimensional structural analysis. RNA 8: 426–439.

Kamath, RS, A. G. Fraser, Y. Dong, G. Poulin, R. Durbin *et al*., 2003 Systematic functional analysis of the *C. elegans* genome using RNAi. Nature 421: 231–237.

Kasturi, P., S. Zanetti, M. Passannante, Z. Saudan, F. Müller *et al*., 2010 The *C. elegans* sex determination protein MOG-3 functions in meiosis and binds to the CSL co-repressor CIR-1. Dev. Biol. 344: 593–602.

Kao, H.-Y., and P. G. Siliciano, 1996 Identification of Prp40, a novel essential yeast splicing factor associated with the U1 small nuclear ribonucleoprotein particle. Mol. Cell. Biol. 16: 960–967.

Keikhaee, M. R., E. B. Nash, S. M. O'Rourke, and B. Bowerman, 2014 A semi-dominant mutation in the general splicing factor SF3a66 causes anterior-posterior axis reversal in one-cell stage *C. elegans* embryos. PLoS One 9: e106484.

Kerins, J. A., M. Hanazawa, M. Dorsett, and T. Schedl, 2010 PRP-17 and the pre-mRNA splicing pathway are preferentially required for the proliferation versus meiotic development decision and germline sex determination in *Caenorhabditis elegans*. Dev. Dyn. 239: 1555–1572.

Kim, S., J. A. Govindan, Z. J. Tu, and D. Greenstein, 2012 SACY-1 DEAD-Box helicase links the somatic control of oocyte meiotic maturation to the sperm-to-oocyte switch and gamete maintenance in *Caenorhabditis elegans*. Genetics 192: 905–928.

Kim, Y. J., and O. Abdel-Wahab, 2017 Therapeutic targeting of RNA splicing in myelodysplasia. Semin. Hematol. 54: 167–173.

Kosinski, M., K. McDonald, J. Schwartz, I. Yamamoto, and D. Greenstein, 2005 *C. elegans* sperm bud vesicles to deliver a meiotic maturation signal to distant oocytes. Development 132: 3357–3369.

Levy, A. D., J. Yang, and J. M. Kramer, 1993 Molecular and genetic analyses of the *Caenorhabditis elegans dpy-2* and *dpy-10* collagen genes: a variety of molecular alterations affect organismal

morphology. Mol. Bio. Cell 4: 803–817.

Lewinsohn, M., A. L. Brown, L. W. Weinel, C. Phung, G. Rafidi *et al.*, 2016 Novel germ line *DDX41* mutations define families with a lower age of MDS/AML onset and lymphoid malignancies. Blood 127: 1017–1023.

Li, R., N. Sobreira, P. D. Witmer, K. W. Pratz, and E. M. Braunstein, 2016 Two novel germline *DDX41* mutations in a family with inherited myelodysplasia/acute myeloid leukemia. Hematologica 101: e228–e231.

Li, X., S. Liu, J. Jiang, S. Espinosa, R. C. Hill *et al*., 2017 CryoEM structure of *Saccharomyces cerevisiae* U1 snRNP offers insight into alternative splicing. Nat. Commun. 8: 1035.

Longman, D., I. L. Johnstone, and J. F. Cáceres, 2000 Functional characterization of SR and SR-related genes in *Caenorhabditis elegans*. EMBO J. 19: 1625–1637.

Maciejewski, J. P., R. A. Padgett, A. L. Brown, and C. Müller-Tidow, 2017 DDX41-related myeloid dysplasia. Semin. Hematol. 54: 94–97.

Maine, E. M., and J. Kimble, 1993 Suppressors of *glp-1*, a gene required for cell communication during development in *Caenorhabditis elegans*, define a set of interacting genes. Genetics 135: 1011–1022.

Maita, H., H. Kitaura, H. Ariga, and S. M. Iguchi-Ariga, 2005 CIR, a corepressor of CBF, binds to PAP-1 and effects alternative splicing. Exp. Cell Res. 303: 375–387.

Mantina, P., L. McDonald, A. Kulaga, L. Zhao, and D. Hansen, 2009 A mutation in *teg-4*, which encodes a protein homologous to the SAP130 pre-mRNA splicing factor, disrupts the balance between proliferation and differentiation in the *C. elegans* germ line. Mech. Dev. 126: 417–429.

Nadarajan, S., J. A. Govindan, M. McGovern, E. J. Hubbard, and D. Greenstein, 2009 MSP and GLP-1/Notch signaling coordinately regulate actomyosin-dependent cytoplasmic streaming and oocyte growth in *C. elegans*. Development 136: 2223–2234.

997 Nishiwaki, K., and J. Miwa, 1998 Mutations in genes encoding extracellular matrix proteins suppress
998 the *emb-5* gastrulation defect in *Caenorhabditis elegans*. Mol. Gen. Genet. 259: 2–12.
999 Novak, P., X. Wang, M. Ellenbecker, S. Feilzer, and E. Voronina, 2015 Splicing machinery facilitates
1000 post-transcriptional regulation by FBFs and other RNA-binding proteins in the *Caenorhabditis*
1001 *elegans* germline. G3 5: 2051–2059.
1002 Omura, H., D. Oikawa, T. Nakane, M. Kato, R. Ishii *et al*., 2016 Structural and functional analysis of
1003 DDX41: a bispecific immune receptor for DNA and cyclic dinucleotide. Sci. Rep. 6: 34756.
1004 Ortiz, M. A., D. Noble, E. P. Sorokin, and J. Kimble, 2014 A new dataset of spermatogenic vs. oogenic
1005 transcriptomes in the nematode *Caenorhabditis elegans*. G3 4: 1765–1772.
1006 Page-McCaw, P. S., K. Amonlirdviman, and P. A. Sharp, 1999 PUF60: a novel U2AF65-related
1007 splicing activity. RNA 5: 1548–1560.
1008 Paix, A., Y. Wang, H. E. Smith, C. Y. Lee, D. Calidas *et al*., 2014 Scalable and versatile genome
1009 editing using linear DNAs with microhomology to Cas9 sites in *Caenorhabditis elegans*.
1010 Genetics 198: 1347–1356.
1011 Papaemmanuil, E., M. Gerstung, L. Bullinger, V. I. Gaidzik, P. Paschka *et al.*, 2016 Genomic
1012 classification and prognosis in acute myeloid leukemia. N. Engl. J. Med. 374: 2209–2221.
1013 Parvatiyar, K., Z. Zhang, R. M. Teles, S. Ouyang, Y. Jiang *et al*., 2012. The helicase DDX41
1014 recognizes the bacterial secondary messengers cyclic di-GMP and cyclic di-AMP to activate a
1015 type I interferon immune response. Nature Immunology 13: 1155–1161.
1016 Pepper, A. S.-R., D. J. Killian, and E. J. A. Hubbard, 2003 Genetic analysis of *Caenorhabditis elegans*
1017 *glp-1* mutants suggests receptor interaction or competition. Genetics 163: 115–132.
1018 Perry, M. D., W. Li, C. Trent, B. Robertson, A. Fire *et a*l., 1993 Molecular characterization of the *her-*
1019 *1* gene suggests a direct role in cell signaling during *Caenorhabditis elegans* sex determination.
1020 Genes Dev. 7: 216–228.

Peters, D., C. Radine, A. Reese, W. Budach, D. Sohn, and R. U. Jänicke, 2017 The DEAD-box RNA helicase DDX41 is a novel repressor of $p21^{WAF1/CIP1}$ mRNA translation. J. Biol. Chem. 292: 8331–8341.

Polprasert, C., I. Schulze, M. A. Sekeres, H. Makishima, B. Przchodzen *et al.*, 2015 Inherited and somatic defects in DDX41 in myeloid neoplasms. Cancer Cell 27: 658–670.

Puoti, A., and J. Kimble, 1999 The Caenorhabditis elegans sex determination gene *mog-1* encodes a member of the DEAH-Box protein family. Mol. Cell Biol. 19: 2189–2197.

Puoti, A., and J. Kimble, 2000 The hermaphrodite sperm/oocyte switch requires the *Caenorhabditis elegans* homologs of PRP2 and PRP22. Proc. Natl. Acad. Sci. USA 97: 3276–3281.

Rodrigues, F., L. Thuma, and C. Klämbt, 2012 The regulation of glial-specific splicing of Neurexin IV requires HOW and Cdk12 activity. Development 139: 1765–1776.

Rose, K. L., V. P. Winfrey, L. H. Hoffman, D. H. Hall, T. Furuta *et al.*, 1997 The POU gene *ceh-18* promotes gonadal sheath cell differentiation and function required for meiotic maturation and ovulation in *Caenorhabditis elegans*. Dev. Biol. 192: 59–77.

Rual, J. F., N. Klitgord, and G. Achaz 2007 Novel insights into RNAi off-target effects using *C. elegans* paralogs. BMC Genomics 8: 106.

Sam, M., W. Wurst, M. Klüppel, O. Jin, H. Heng *et al*., 1998 *Aquarius*, a novel gene isolated by gene trapping with an RNA-dependent RNA polymerase motif. Dev. Dyn. 212: 304–317.

Sanchez, P., K. J. Daniels, Y. N. Park, and D. R. Soll 2014 Generating a battery of monoclonal antibodies against native green fluorescent protein for immunostaining, FACS, IP, and ChIP using a unique adjuvant. Monoclon Antib Immunodiagn Immunother. 33: 80–88.

Schedl, T., and J. Kimble, 1988 *fog-2*, a germ-line-specific sex determination gene required for hermaphrodite spermatogenesis in *Caenorhabditis elegans*. Genetics 119: 43–61.

Schneider, M., H.-H. Hsiao, C. L. Will, R. Giet, H. Urlaub *et al*., 2010 Human PRP4 kinase is required for stable tri-snRNP association during spliceosomal B complex formation. Nat. Struct. Mol.

Biol. 17: 216–221.

Schütz, P., T. Karlberg, S. van den Berg, R. Collins, L. Lehtiö *et al*., 2010 Comparative structural analysis of human DEAD-box RNA helicases. PLoS One 5: e12791.

Sébert, M., M. Passet, A. Raimbault, R. Rahmé, E. Raffoux *et al*., 2019 Germline *DDX41* mutations define a significant entity within adult MDS/AML patients. Blood 134: 1441–1444.

Seiler, M., A. Yoshimi, R. Darman, B. Chan, G. Keaney *et al*., 2018 H3B-8800, an orally available small-molecule splicing modulator, induces lethality in spliceosome-mutant cancers. Nat. Med. 24: 487–504.

Serrat, X., D. Kukhtar, E. Cornes, A. Esteve-Codina, H. Benlloch et. Al., 2019 CRISPR editing of *sftb-1/SF3B1* in *Caenorhabditis elegans* allows the identification of synthetic interactions with cancer-related mutations and the chemical inhibition of splicing. PLoS Genetics 15: e1008464.

Spike, C. A., D. Coetzee, C. Eichten, X. Wang, D. Hansen *et al*., 2014a The TRIM-NHL protein LIN-41 and the OMA RNA-binding proteins antagonistically control the prophase-to-metaphase transition and growth of *Caenorhabditis elegans* oocytes. Genetics 198: 1535–1558.

Spike, C. A., D. Coetzee, Y. Nishi, T. Guven-Ozkan, M. Oldenbroek *et al*., 2014b Translational control of the oogenic program by components of OMA ribonucleoprotein particles in *Caenorhabditis elegans*. Genetics 198: 1513–1533.

Stavrou, S., A. N. Aguilera, K. Blouch, and S. R. Ross, 2018 DDX41 recognizes RNA/DNA retroviral reverse transcripts and is critical for in vivo control of murine leukemia virus infection. MBio 9: e00923–18.

Stavrou, S., K. Blouch, S. Kotla, A. Bass, and S. R. Ross, 2015 Nucleic acid recognition orchestrates the anti-viral response to retroviruses. Cell Host Microbe 17: 478–488.

Sun, L., J. Wu, F. Du, X. Chen, and Z. J. Chen, 2013 Cyclic GMP-AMP synthase is a cytosolic DNA sensor that activates the type I interferon pathway. Science 339: 786–791.

Tefferi, A., and J. W. Vardiman, 2009 Myelodysplastic syndromes. N. Engl. J. Med. 361: 1872–1885.

Timmons, L., and A. Fire, 1998 Specific interference by ingested dsRNA. Nature 395: 854.

Tsukamoto, T., M. D. Gearhart, C. A. Spike, G. Huelgas-Morales, M. Mews *et al.*, 2017 LIN-41 and OMA ribonucleoprotein complexes mediate a translational repression-to-activation switch controlling oocyte meiotic maturation and the oocyte-to-embryo transition in *Caenorhabditis elegans*. Genetics 206: 2007–2039.

Van Buskirk, C., and T. Schüpbach, 2002 *half pint* regulates alternative splice site selection in *Drosophila*. Developmental Cell 2: 343–353.

Wahl, M. C., C. L. Will, and R. Lührmann, 2009 The spliceosome: design principles of a dynamic RNP machine. Cell 136: 701–718.

Wang, C., L. Wilson-Berry, T. Schedl, and D. Hansen, 2012 TEG-1 CD2BP2 regulates stem cell proliferation and sex determination in the *C. elegans* germ line and physically interacts with the UAF-1 U2AF65 splicing factor. Dev. Dyn 241: 505–521.

Will. C. L., H. Urlaub, T. Achsel, M. Gentzel, M. Wilm *et al*., 2002 Characterization of a novel SF3b and 17S U2 snRNP proteins, including a human Prp5p homologue and an SF3b DEAD-box protein. EMBO J. 18: 4978–4988.

Yoshida, K., M. Sanada, Y. Shiraishi, D. Nowak, Y. Nagata *et al*., 2011 Frequent pathway mutations of splicing machinery in myelodysplasia. Nature 478: 64–69.

Yoshida, K., and S. Ogawa, 2014 Splicing factor mutations and cancer. WIREs RNA 5: 445–459.

Yoshimi, A., K.-T. Lin, D. H. Wiseman, M. A. Rahman, A. Pastore *et al*., 2019 Coordinated alterations in RNA splicing and epigenetic regulation drive leukaemogenesis. Nature 574: 273–277.

Zanetti, S., and A. Puoti, 2013 Sex determination in the *Caenorhabditis elegan*s germline. Adv. Exp. Med. Biol. 757: 41–69.

Zanetti, S., M. Meola, A. Bochud, and A. Puoti, 2011 Role of the *C. elegans* U2 snRNP protein MOG-2 in sex determination, meiosis, and splice site selection. Dev. Biol. 354: 232–241.

Zhang, L., J. D. Ward, Z. Cheng, and A. F. Dernburg, 2015 The auxin-inducible degradation (AID) system enables versatile conditional protein depletion in *C. elegans*. Development 142: 4374–4384.

Zhang, X., C. Yan, J. Hang, L. I. Finci, J. Lei *et al.*, 2017 An atomic structure of the human spliceosome. Cell 169: 918–928.

Zhang, Z., B. Yuan, M. Bao, N. Lu, T. Kim *et al*., 2011 The helicase DDX41 senses intracellular DNA mediated by the adaptor STING in dendritic cells. Nature Immunol. 12: 959–965.

Table 1 RNAi of *sacy-1* enhancer loci increase the penetrance of germline or lethal phenotypes in *sacy-1(tn1385)* reduction-of-function mutants

RNAi[a]	Genotype	Sterile (%)[b]	Gamete degeneration[b] (%)	Embryonic lethal (%)[c]
L4440 (control)	Wild type	0 (n=338)	0 (n=338)	1 (n=674)
	sacy-1(tn1385)	0 (n=256)	0 (n=256)	1 (n=502)
mog-2 (II-3D16)	Wild type	4 (n=172)	0 (n=54)	7 (n=574)
	sacy-1(tn1385)	43 (n=254)	47 (n=72)	95 (n=426)
Y111B2A.25 (III-6G22)	Wild type	22 (n=230)	1 (n=94)	84 (n=463)
	sacy-1(tn1385)	95 (n=272)	16 (n=110)	93 (n=42)
cacn-1[d] (II-9E09)	Wild type	100 (n=164)	35 (n=40)	ND
	sacy-1(tn1385)	100 (n=224)	81 (n=52)	ND
emb-4 (V-12E12)	Wild type	2 (n=184)	0 (n=110)	12 (n=337)
	sacy-1(tn1385)	89 (n=176)	42 (n=82)	N.D.
emb-4 (V-12E14)	Wild type	4 (n=288)	0 (n=96)	13 (n=421)
	sacy-1(tn1385)	91 (n=202)	80 (n=120)	ND
emb-4 (V-12E16)	Wild type	4 (n=210)	0 (n=96)	9 (n=433)
	sacy-1(tn1385)	91 (n=326)	87 (n=140)	ND

[a]RNAi clones showing genetic interactions with *sacy-1* are listed with the target gene name in italics and the location of the clone in the RNAi library in parentheses. The identity of clones was verified by DNA sequencing.

[b]Sterility and gamete degeneration were scored by DIC microscopy on the first day of adulthood 24 hours post-L4 at 22°C. Gonad arms were scored as sterile if they did not produce embryos and exhibited defects in gametogenesis. Number of gonad arms scored is reported.

[c]Embryonic lethality was measured by conducting daily egg lays over the reproductive lifespan and determining the number of embryos that failed to hatch by 48 hours after egg laying. The number of embryos scored is reported.
[d]*cacn-1* was not initially identified as an enhancer of *sacy-1* during the genome-wide RNAi screen because *cacn-1(RNAi)* results in complete sterility in both *sacy-1(tn1385)* and wild-type animals. However, we determined that RNAi to the *Y111B2A.25* pseudogene likely targets *cacn-1* (see text for details).
ND, not determined.

Table 2 Genetic interactions between *sacy-1* and *emb-4*

A. Enhancement of germline and somatic *sacy-1* mutant defects

Genotype	Vulval rupture (%)	Sterile and Pvl[a] (%)	Sterile[a] (%)	Fertile (%)
sacy-1(tm5503) (n=284)	3	1	96	0
sacy-1(tm5503)/+; emb-4(sa44)[b] (n=205)	0	0	0	100
sacy-1(tm5503); emb-4(sa44)[b] (n=242)	83	16	1	0
sacy-1(tn1385) (n=278)	0	0	0	100
sacy-1(tn1385)/+; emb-4(sa44)[b] (n=201)	0	0	0	100
sacy-1(tn1385); emb-4(sa44)[b,c] (n=144)	36	4	3	57[d]

[a]Sterile animals exhibit the *sacy-1(lf)* gamete degeneration phenotype.

[b]The *hT2(qIs48)* balancer chromosome, which is dominantly marked with GFP, was used to differentiate between *sacy-1(tm5503)* heterozygotes and homozygotes.

[c]The progeny of *sacy-1(tn1385)/hT2(qIs48); emb-4(sa44)* hermaphrodites; the balancer chromosome provides maternal *sacy-1(+)* function. The fertile F1 progeny of these animals are maternal-effect lethal, see Table 2B, below.

[d]These adult hermaphrodites produce a majority of embryos that fail to hatch, see Table 2B.

B. Enhancement of embryonic lethality

Genotype[a]	Embryonic lethal (%)	L1 lethal (%)	Viable (%)
sacy-1(tn1385) (n=949)	1	0	99
emb-4(sa44) (n=1348)	4	0	96
sacy-1(tn1385); emb-4(sa44)[b] (n=620)	97	3	0

[a]The number of embryos examined.

[b]The F1 progeny of fertile *sacy-1(tn1385); emb-4(sa44)* parents derived from the *sacy-1(tn1385)/+; emb-4(sa44)* heterozygotes analyzed in Table 2A above.

Table 3. Spliceosomal proteins associated with SACY-1 using tandem affinity purification

		Protein Coverage (%)[a]	
		Experiment I	Experiment II
Protein		Tandem IP female background[b]	Tandem IP hermaphrodite background[b]
SACY-1	DDX41/Abstrakt/recruited to C-complex	78.9	76.5
Spliceosomal proteins	Human protein/Spliceosome subcomplex		
PRP-19	PRP19hPRP19/CDC5L complex[c]	62.0	55.5
MOG-2[d]	U2A'/17S U2 snRNP[c]	56.1	42.3
SKP-1	SNW1/SKIP/hPRP19/CDC5L-related complex	52.9	40.9
EMB-4, isoform b	Aquarius/KIAA0560/Intron-binding complex RNA helicase[c, e]	50.4	30.6
PRP-17	hPRP17/WD40-domain step 2 factor[c, f]	48.3	33.7
CYN-13	Cyclophilin E/PPIE/Intron-binding	46.8	37.8

	complex[e]		
CDC-5L	CDC5L/hPRP19/CDC5L complex[c]	45.8	26.2
Y69A2AR.21	CCDC12/Recruited to B-complex[c]	45.6	52.1
RBM-22	RBM22/ hPRP19/CDC5L-related complex[c, g]	45.1	43.9
EFTU-2[d]	U5 116K[c]	45.1	37.2
ISY-1	hIsy1/Intron-binding complex[e]	40.8	34.8
PLRG-1	PLRG1/PRL1/hPRP19/CDC5L complex[c]	39.1	27.3
RBMX-2[d]	CGI-79/SNU17/IST3/hRes complex[c]	38.7	20.9
CYN-10	PPIL3b/peptidyl-prolyl isomerase recruited to C-complex[c]	37.9	23.6
RBM-25	RBM25/affects alternative splicing/putative U1 snRNP component	37.5	25.8
RNP-6, isoform a	PUF60/U2AF65-related promotes alternative splicing[h]	37.2	49.3
SYF-2	GCIP p29/SYF2/Recruited to C-complex[c]	37.2	29.9

PRP-8	PRPF8/PRP8/U5 220K[i]	37.0	29.4
EMB-4, isoform a	Aquarius/KIAA0560/Intron-binding complex RNA helicase[c, d]	36.8	28.6
DDX-35	DDX35/DHX35/Recruited to C-complex[c]	36.8	19.8
SNRP-40.1	snRNP40/U5 40K[c]	36.6	27.5
RBM-39[d]	RBM39/protein recruited to A-complex[c]	35.9	31.0
CACN-1	Cactin/C-complex[c, j]	35.9	13.4
ACIN-1	Acinus/Exon junction complex[c]	35.2	13.1
M03F8.3	hSYF3/CRNKL1/hPRP19/CDC5L-related protein	35.0	24.3
ZK1098.1	PRP40/FBP11[k]	34.5	28.7
C50D2.5	SF3b14/SF3b6/17S U2 snRNP protein	33.3	8.7
SYF-1	hSyf1/Xab2/Intron-binding complex[e]	32.4	28.0
EMB-4, isoform e	Aquarius/KIAA0560/Intron-binding complex RNA helicase[c, e]	31.7	18.4
F33D11.10	EIF4A3/ Exon junction complex[c]	31.3	17.0

REPO-1	SF3a66/SF3A2/17S U2 snRNP protein[c, l]	30.6	5.9
Y54G2A.12	hPRP17/hCDC40/Step 2 factor	29.9	27.7
PNN-1	Pinin/Exon junction complex[c]	28.7	20.3
BCAS-2	Spf27/BCAS2/hPRP19/CDC5L complex[c]	28.6	20.2
EMB-4, isoform d	Aquarius/KIAA0560/Intron-binding complex RNA helicase[c, e]	28.3	27.9
RSP-7	p54 SR protein[m]	27.2	27.4
CWC-15	CCAP2/CWC15/hPRP19/CDC5L complex[c]	27.0	22.6
LET-858	KIAA1604/CWC22/Recruited to B-complex[c]	26.5	16.5
R07E5.1	GPATCH1/ECGP[n]	26.0	11.2
RSR-2	SRm300/SRRM2	24.0	21.2
MOG-3	CCDC49/CWC25/recruited to C-complex[o]	21.3	20.0
CYN-12	PPIL1/ peptidyl-prolyl isomerase/hPrp19/CDC5L-related protein	20.1	20.1

F25B4.5	PRPF39/PRP39/U1 snRNP auxiliary protein[p]	20.1	10.0
SNRP-40.2	U5 snRNP 40K[c]	19.6	16.0
C16C10.4	SAP18/Exon junction complex[c]	17.5	7.8
DDX-23	U5 snRNP 100K/PRP28[c]	17.1	7.5
R08D7.1	BUD13/hRes complex[c]	16.6	3.7
TEG-4	SF3b130/SF3B3/17S U2 snRNP[c]	14.9	8.8
SFTB-1[s]	SF3b155/SF3B1/17S U2 snRNP[c]	14.7	1.2
F53H1.1, isoform a	SF3b125/17S U2 snRNP[q]	14.5	3.4
RNP-6, isoform b	PUF60/U2AF65-related promotes alternative splicing[h]	13.6	20.3
PRPF-4, isoform a	PRP4 kinase[r]	12.5	7.1
RNP-3	U2B''/17S U2 snRNP[c]	12.4	12.4
F53H1.1, isoform e	SF3b125/17S U2 snRNP[q]	11.9	5.1
PRP-21	SF3a120/SF3A1/PRP21/17S U2 snRNP protein[c]	11.8	7.0
SNRP-200[d]	U5 200K[c]	11.1	7.7
SFTB-2	SF3b145/SF3B2/17S U2 snRNP[c]	10.1	1.5

RNP-5	RNPS1/EJC[c]	10.0	18.0

[a]Peptide coverage in a single gel slice assessed by mass spectrometry in the various SACY-1 purifications from DG4068 *sacy-1(tn1632[3x flag::PreScission::gfp::tev::s::sacy-1]) fog-1(q253)* extract and DG4070 *sacy-1(tn1632)* extract. Only proteins showing at least 10% coverage in the tandem immunopurification (IP) from the high-speed supernatant are shown. The complete data on which Table 3 is based, including filtering criteria, are presented in File S1.

[b]Experiments I and II utilized 515 mg and 280 mg total protein, respectively, from a high-speed supernatant for tandem IP.

[c]Bessonov *et al*. 2008.

[d]MOG-2, EFTU-2, RBMX-2, RBM-39, SFTB-1, TEG-4 and SNRP-200 are reported in Table 3 and not filtered out despite their low representation (14.2%, 4.4%, 3.6%, 6.9%, 2.0%, 1.1% and 4.5% coverage, respectively) in the LIN-41 tandem IP from high-speed supernatant (Tsukamoto *et al*. 2017) because they were reported as splicing factors. F33D11.10 is reported in Table 3 despite its low representation (10.3% coverage) in the OOC-5 tandem IP from high-speed supernatant (unpublished data) because it was reported as a splicing factor.

[e]De *et al.* 2015; Haselbach *et al*. 2018.

[f]Bertram *et al*. 2017.

[g]Zhang *et al*. 2017.

[h]Page-McCaw *et al*. 1999; Van Buskirk and Schüpbach 2002; Hastings *et al*. 2007.

[i]Grainger and Beggs 2005.

Fica *et al*. 2019.

[k]Kao and Siliciano 1996.

[l]Keikhaee *et al*. 2014.

[m]Chaudhary *et al*. 1991; Longman *et al*. 2000.

[n]Bessonov *et al*. 2010.

[o]Fabrizio *et al*. 2009.

[p]Li *et al*. 2017.

[q]Will *et al*. 2002.

[r]Schneider *et al*. 2010.

Table 4 *sacy-1(tn1385*rf) enhances the *glp-1(ar202)* Tumorous phenotype

Strain	Gonad arms containing mitotic undifferentiated germ cells in the proximal gonad arm[a]
sacy-1(tn1385[G533R]*)*	0 (n=256)[b]
glp-1(ar202)	0.8 (n=364)[b]
sacy-1(tn1385[G533R]*); glp-1(ar202)*	49.6 (n=415)[b]
sacy-1(tn1887[R534H]*); glp-1(ar202)*	0 (n=62)

[a]The percentage of young adult hermaphrodites were examined by DIC microscopy approximately 40 hours post-L4 at 15°C. The number of gonad arms scored is listed.

[b]In addition, dissected and fixed gonad from the same stage were stained for the phosphohistone H3(Ser10) M-phase marker. Of 25 *sacy-1(tn1385); glp-1(ar202)* gonads scored, 16 (64%) contained phosphohistone H3-positive undifferentiated germ cells in the proximal gonad arm. The average number of proximal phosphohistone H3-positive germ cells in the Tumorous gonads was 22 ± 12. None of the *sacy-1(tn1385)* (n=18) or *glp-1(ar202)* (n=31) dissected gonads examined contained phosphohistone H3-positive undifferentiated germ cells in the proximal gonad arm.

1174 **Table 5 *sacy-1* alleles relevant to this study**

Allele	Alteration	Phenotypes	Inferred activity
Loss-of-function alleles			
sacy-1(tm5503)[a]	619 bp deletion	Sterile, gamete degeneration	Likely null
sacy-1(tn1615)[b]	10 bp deletion	Sterile, gamete degeneration	Likely null
sacy-1(tn1385)[a]	G533R	Viable and fertile, suppresses *acy-4* sterility, suppresses *fog-2* sterility	Reduction of function
sacy-1(tn1391)[a]	G473R	Viable and fertile, supresses *acy-4* sterility, suppresses *fog-2* sterility	Reduction of function
sacy-1(tn1440)[a]	G331R	Viable and fertile, suppresses *acy-4* sterility, suppresses *fog-2* sterility	Reduction of function
sacy-1(tn1482)[b]	D506N	Viable and fertile, suppresses *fog-2* sterility[c]	Reduction of function
sacy-1(tn1483)[b]	G269E	Viable and fertile, suppresses *fog-2* sterility[c]	Reduction of function
Alleles with antagonistic activity			
sacy-1(tn1479)[b]	G504E	Sterile, adult lethal (rupture) or gamete degeneration	*sacy-1(tn1479)*[b]
sacy-1(tn1480)[b]	H527Y	Viable and fertile at 20°C and suppresses *fog-2*	Loss of function with antimorphic activity,

		sterility.[c] Embryonic lethal or larval arrest at 15°C. Sterile and spermatogenesis-defective at 25°C	dominant Him
sacy-1(tn1481)[b]	P222L	Sterile, masculinization of germline	Recessive gain-of-function Loss of function with antimorphic activity
sacy-1(tn1887)[b]	R534H	Viable and fertile.	Weak antagonistic activity; enhances the dominant Him phenotype of *sacy-1(tn1480)*

[a]Kim *et al*. 2012.

[b]This work.

[c]Suppression of *acy-4* sterility was not tested.

Table 6 *sacy-1* mutant alleles with antagonistic activity

Allele	Class	Gamete Degeneration[a]	Vulval Rupture[a]	Mog[a,b]	T[c]
sacy-1(tm5503) (n=143)	Strong loss-of-function	5.6	94.4	0	15
sacy-1(tm5503) (n=96)	Strong loss-of-function	96.9	3.1	0	20
sacy-1(tm5503) (n=106)	Strong loss-of-function (from *tm5503/+*)	98.0	2.0	0	25
sacy-1(tm5503)[d] (n=231)	Strong loss-of-function (from *tm5503/tn1480*)	14.7	85.3	0	25
sacy-1(tn1615) (n=92)	Strong loss-of-function	97.8	2.2	0	20
sacy-1(tn1479) (n=170)	Strong loss-of-function with antagonistic activity	11.2	88.8	0	20
sacy-1(tn1481) (n=125)	Recessive gain-of-function	0	0	100	20

[a]The percentage of adult hermaphrodites exhibiting the reported phenotype is shown. Adults were scored 24 hr post-L4 at 20° or 25°C or 48 hr post-L4 at 15°C.

[b]*sacy-1(tn1481)* adult hermaphrodites produce large numbers of sperm but no oocytes and are sterile.

[c]Growth temperature in °C.

[d]The *sacy-1(tm5503)* progeny of *sacy-1(tm5503)/unc-13(e1091) sacy-1(tn1480)* hermaphrodites grown at 25°C.

1185

LEGENDS TO FIGURES

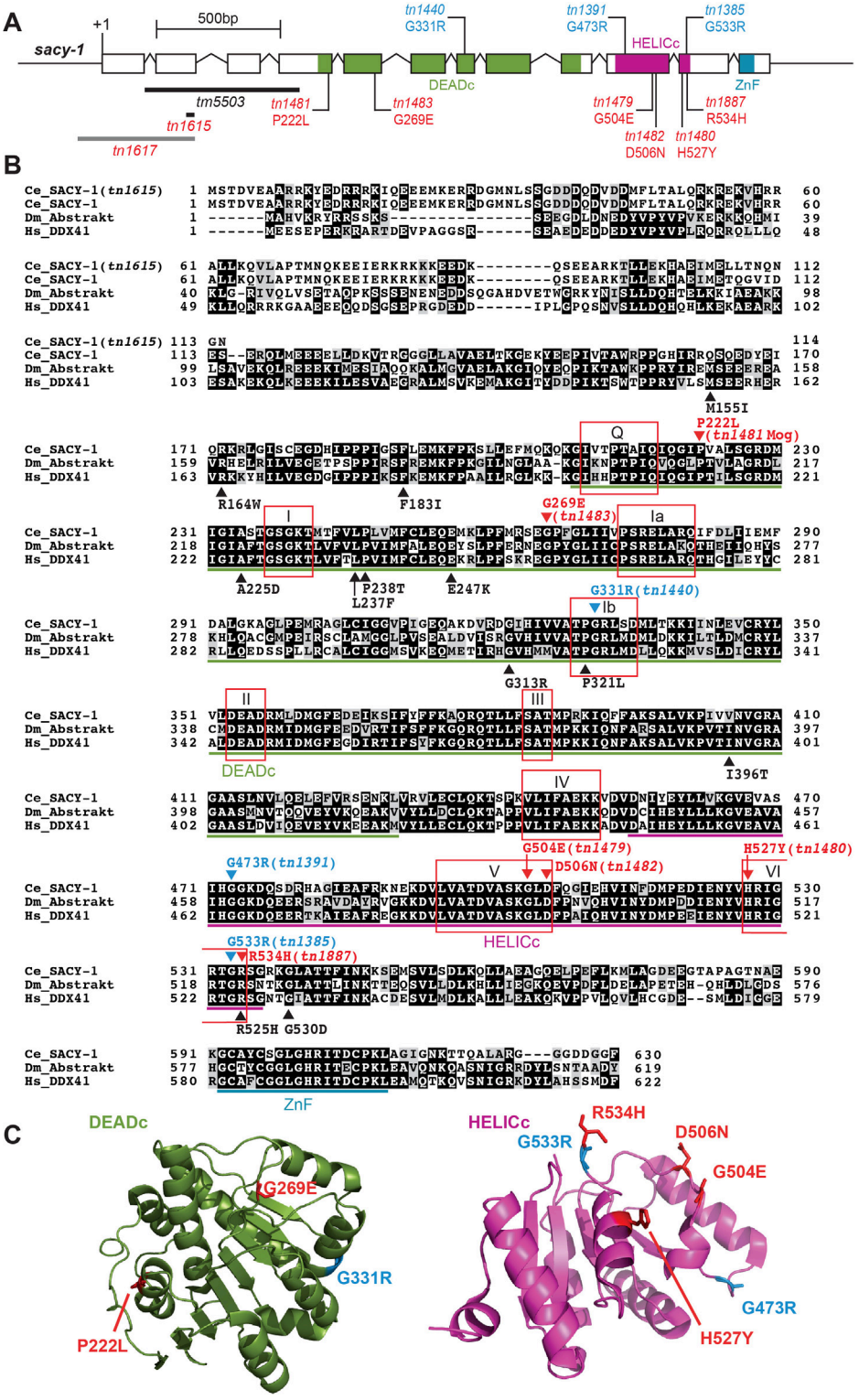

1186

1187 **Figure 1** (A) The structure of *sacy-1*. Newly isolated mutations reported in this study are displayed in

1188 red font beneath the exons. The mutations in blue font shown above the exons were reported

previously (Kim *et al*. 2012). The extent of two deletions, *tm5503* and *tn1615*, that result in *sacy-1* null mutations are shown with black bars. A third deletion, *tn1617*, which is a reduction-of-function mutation, is shown with a gray bar. (B) A protein sequence alignment of SACY-1 (NP_491962.1), Drosophila Abstract (NP_524220.1), and human DDX41 (NP_057306.2). Mutations isolated in *C. elegans* are shown above that sequence, whereas the human mutations associated with myelodysplastic syndromes are shown beneath the human sequence. Conserved domains [DEAD-box domain (DEADc), helicase domain (HELICc), and zinc finger domain (ZnF)] and motifs (Q, I Ia, Ib, III, IV, V, and VI) are indicated as described by Henn *et al*. (2012). (C) The locations of SACY-1 missense mutations are shown on structures of the DDX41 DEADc (Omura *et al*. 2016) and HELICc (Schütz *et al*. 2010) domains. The side chains of the amino acids in the human structure are labeled with amino acid numbering that corresponds to the SACY-1 missense mutations in this study.

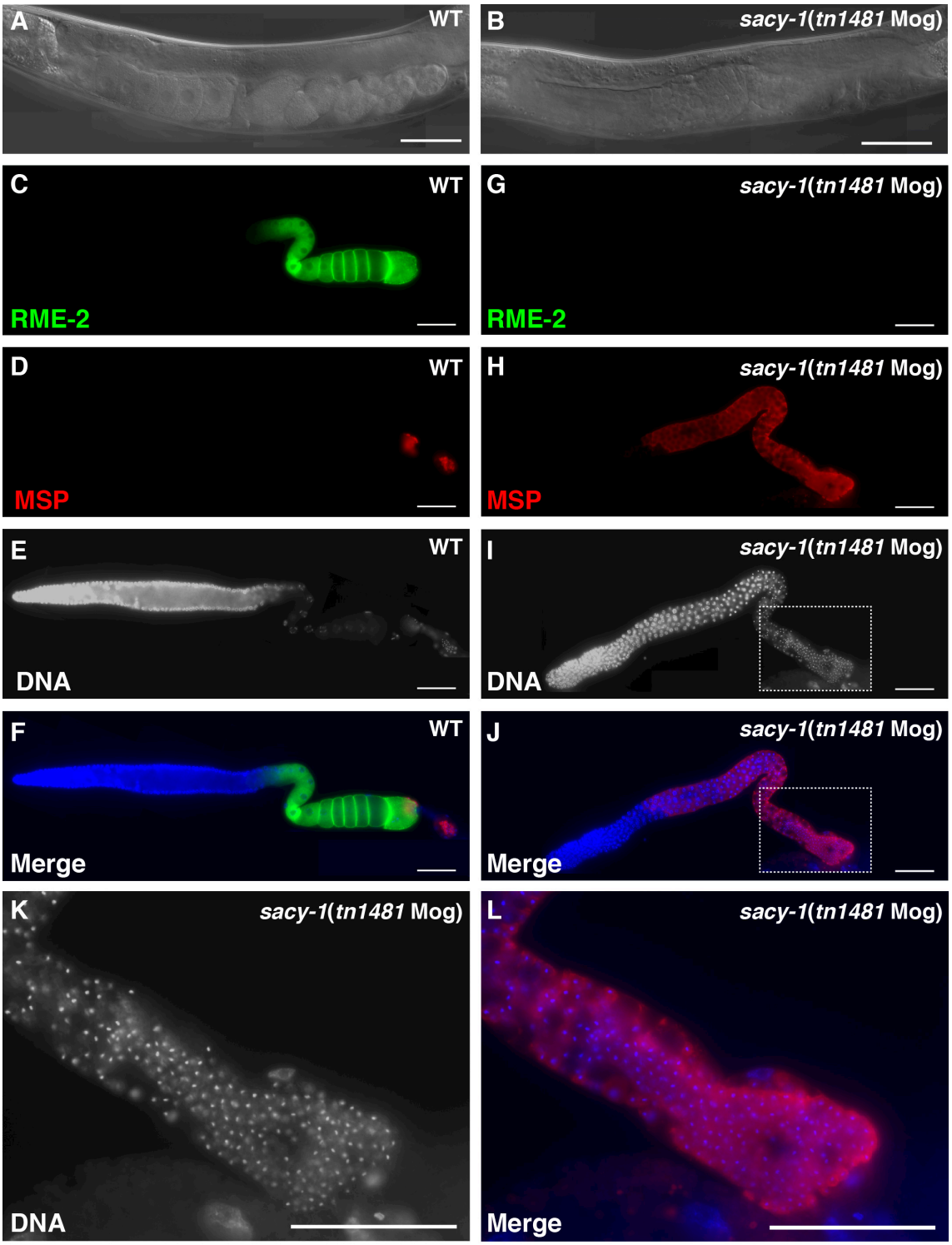

Figure 2 *sacy-1(tn1481)* adult hermaphrodites exhibit a masculinization of germline (Mog) sterile phenotype. DIC images of wild-type (A) and *sacy-1(tn1481)* (B) adult hermaphrodites. The wild-type animal contains oocytes and sperm and produces embryos but the *sacy-1(tn1481)* animal only produces sperm (arrow). (C–L) Dissected gonads stained for the RME-2 yolk receptor (C, G), the

major sperm protein (D, H), or DNA (E, I, and K). Merged images are also shown (F, J, and L). The *sacy-1(tn1481)* mutant overproduces sperm to the exclusion of oocytes and is sterile. This phenotype is completely penetrant. Bars, 50 μm.

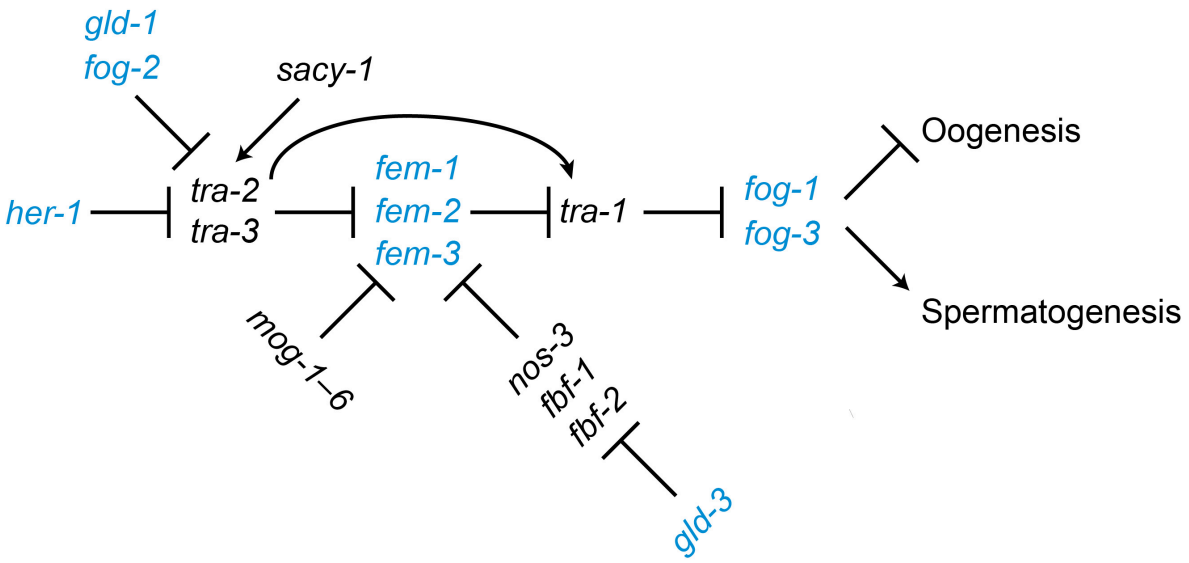

Figure 3 The *C. elegans* germline sex determination pathway. Genes promoting the male and female fate are shown in blue and black, respectively. *sacy-1* promotes the oocyte fate antagonistically to *fog-2*, which promotes spermatogenesis.

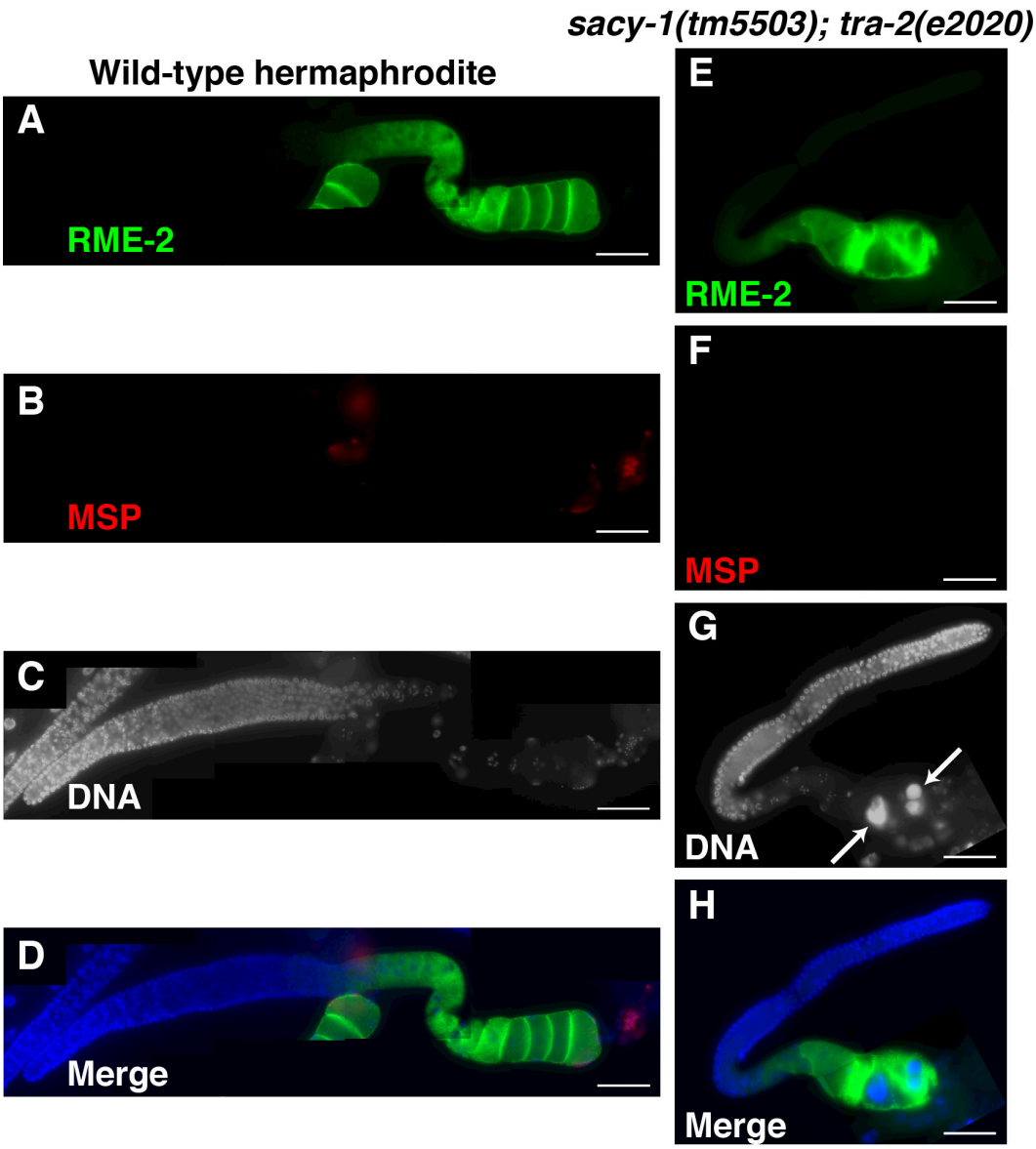

Figure 4 Genetic interactions between *sacy-1* and *tra-2* in germline sex determination were analyzed by combining the strong germline-feminizing dominant *tra-2(e2020)* mutation with the *sacy-1(tm5503)* null mutation. Dissected gonads of wild-type hermaphrodites (A–D) and *sacy-1(tm5503); tra-2(e2020)* females were analyzed by staining for the oocyte RME-2 yolk receptor (A and E) and the major sperm protein (B and F). DNA was detected with DAPI (C and G). Merged images are also shown (D and H). Note gonads from *sacy-1(tm5503); tra-2(e2020)* females do not express MSP and frequently contain endomitotic oocytes (arrows). Bars, 50 µm.

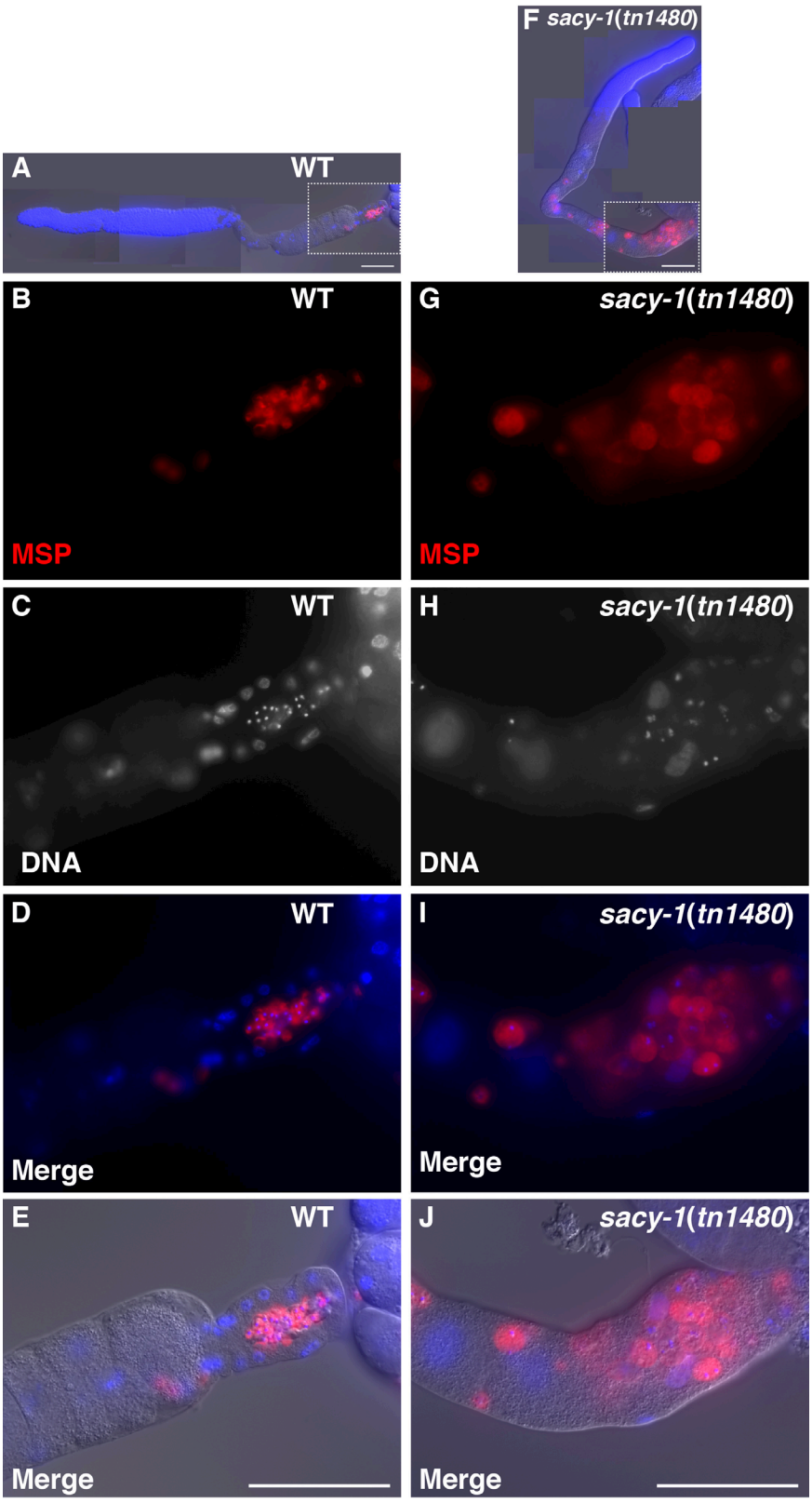

Figure 5 Sperm-defective phenotype of *sacy-1(tn1480)* at 25°C. Dissected gonads of wild-type (A–E) and *sacy-1(tn1480)* (F–J) stained with anti-MSP antibodies (B, G) and DAPI to detect DNA (C, H).

Merged images are also shown (A, D, E, F, I, and J). At 25°C, *sacy-1(tn1480)* hermaphrodites produce swollen and abnormal sperm, which are incapable for fertilization. Note that defective sperm are also found near the bend region in *sacy-1(tn1480)* adults (F) indicating that there is a defect in the sperm-to-oocyte switch. Bars, 50 μm.

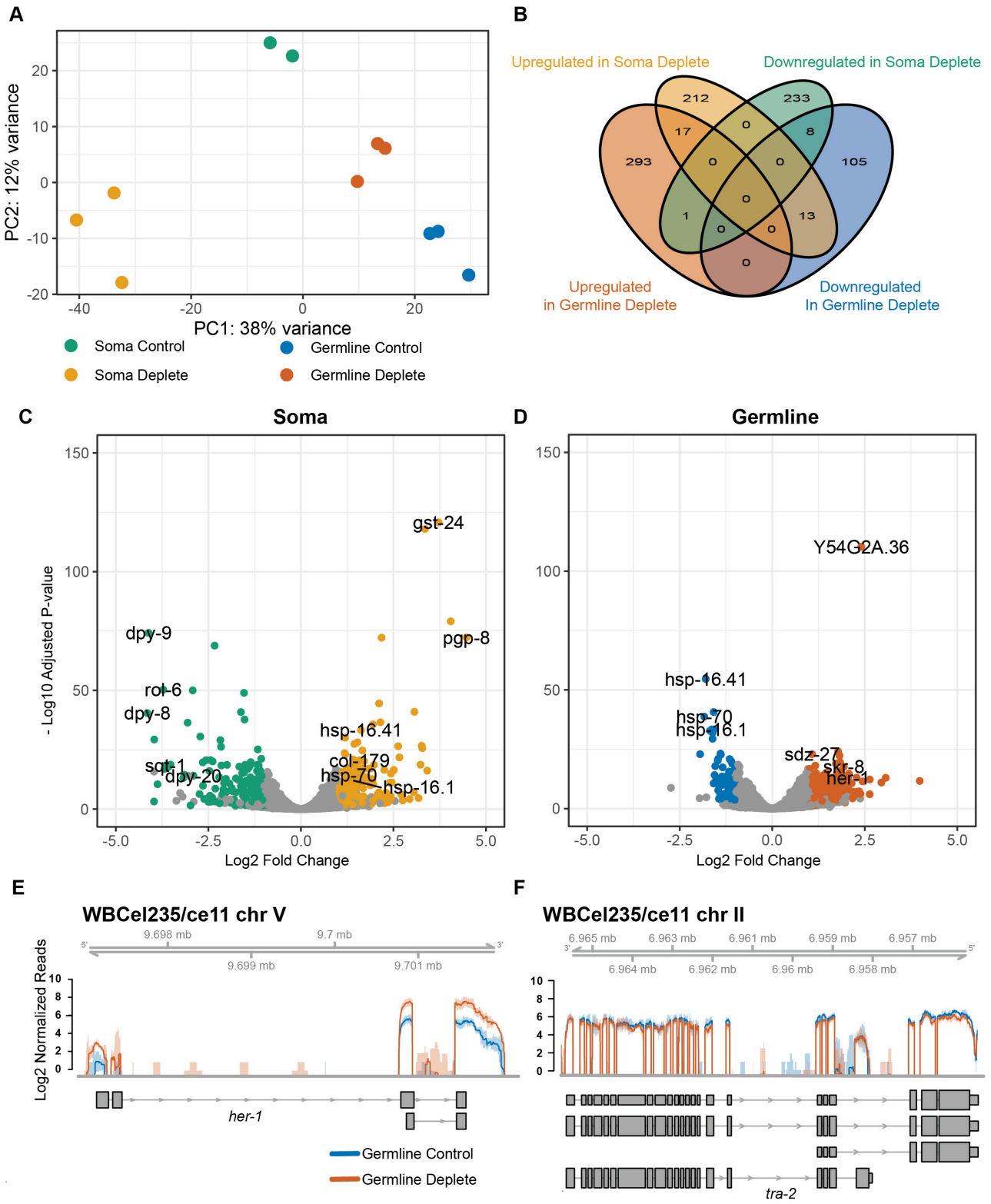

Figure 6 Transcriptome changes upon SACY-1 depletion. (A) PCA comparison of RNA-seq data of controls strains and the experimental samples in which SACY-1 was depleted in the germline or soma, as indicated. Three biological replicates were analyzed for each sample; however, one of the control

samples for the soma depletion exhibited evidence of RNA degradation and was excluded from the analysis. (B) A Venn diagram showing the limited overlap of upregulated genes (2-fold; adjusted $p<0.05$, FPKM deplete > 2.5 and mean counts > 25) and downregulated (2-fold; adjusted $p<0.05$, FPKM control > 2.5 and mean counts > 25) genes in the RNA-seq datasets. (C, D) Volcano plots showing the log2 fold change in expression versus the -log10 of the adjusted p value of genes following SACY-1 depletion in the soma (C) or germline (D). (E, F) The normalized coverage of sequencing reads across *her-1* (E) and *tra-2* (F) following depletion of SACY-1 in the germline. The solid lines represent the mean of the biological replicates and shaded regions represent the corresponding confidence interval. Note, the pattern of *tra-2* splicing is not affected.

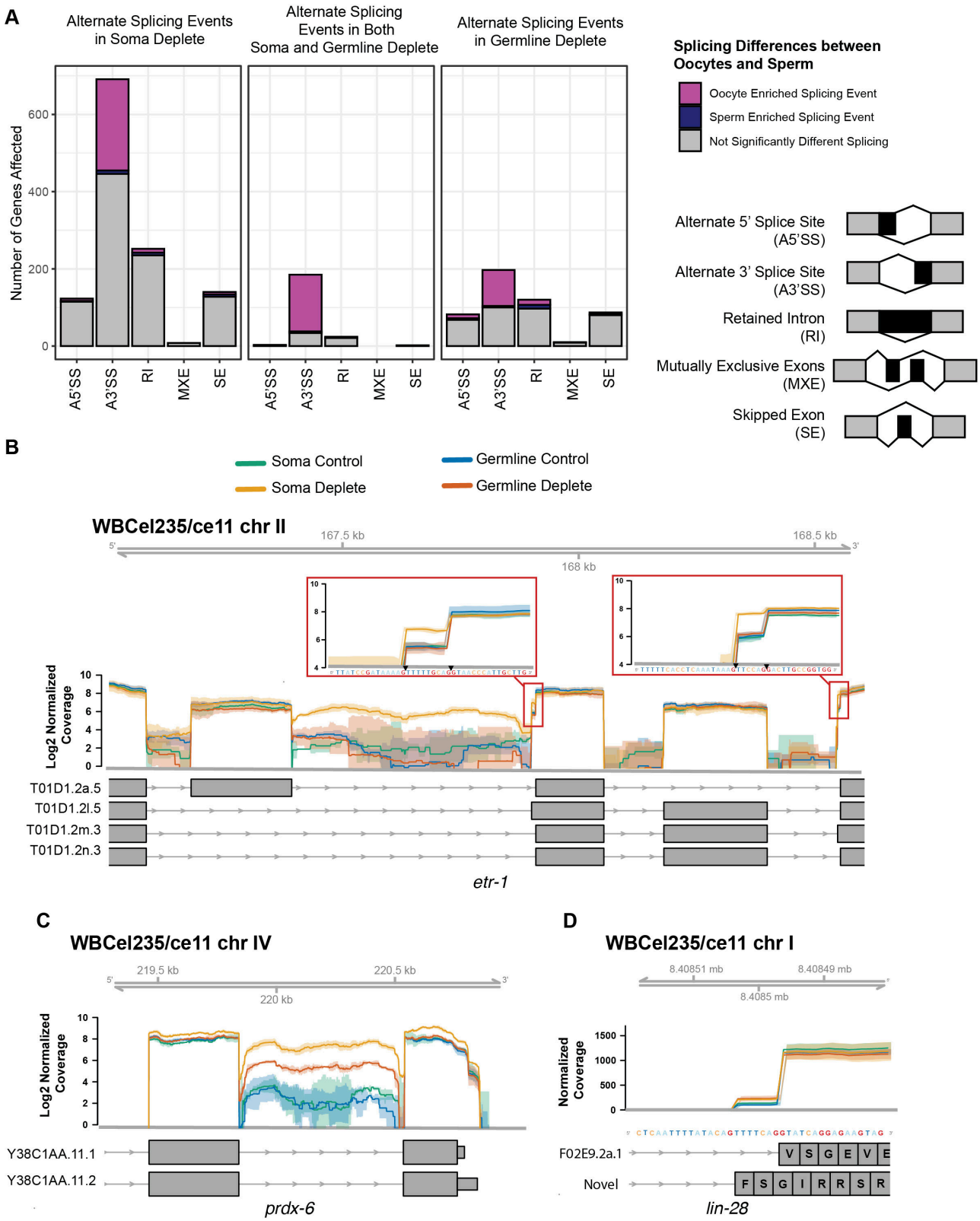

Figure 7 Quantification of altered splicing patterns upon SACY-1 depletion. (A) Bar graphs showing the number of genes with statistically significant (FDR<0.05) changes in splicing patterns. The legend

at the right depicts the nature of the observed splicing changes: A5'SS= Alternate 5' Splice Site, A3'SS = Alternate 3' Splice Site, RI= Retained Intron, MXE=Mutually Exclusive Exons, SE=Skipped Exon (B–D) Examples of alterations in splicing patterns following SACY-1 depletion in the germline or soma as indicated. The *etr-1* gene shows pronounced intron retention and two alternatively spliced 3' sites in the SACY-1 soma depleted (gold) sample (B). A subset of *etr-1* transcript annotations are shown. The *prdx-6* gene has a retained intron in the SACY-1 soma depleted (gold) and germline depleted (red) samples (C). The soma and germline depleted samples have an increase in the usage of alternate splice acceptor in the *lin-28* gene that results in an altered reading frame (D). The solid lines represent the mean of the biological replicates and shaded regions represent the corresponding confidence interval.